Self-organized kilometre-scale shoreline sandwave generation: sensitivity to model and physical parameters

Déborah Idier[1], Albert Falqués[2], Jérémy Rohmer[1], Jaime Arriaga[2]

Corresponding author: D. Idier, BRGM, avenue Claude Guillemin, 45060 Orléans cédex, France. (d.idier@brgm.fr)

[1]BRGM, Orléans Cédex, France.

[2]Department of Applied Physics, Universitat Politècnica de Catalunya (UPC), Barcelona, Catalonia, Spain.

Key Points.

- Sandwaves under low-angle waves are favoured by bathymetric undulations that are more pronounced than the associated shoreline undulations.
- Large wave angle, large closure depth and small wave period favour shoreline sandwave formation.
- A statistical model for the probability that the critical angle for instability equals $\sim 42°$ is set up.

Abstract. The instability mechanisms for self-organized kilometre-scale shoreline sandwaves have been extensively explored by modelling. However, while the assumed bathymetric perturbation associated with the sandwave controls the feedback between morphology and waves, its effect on the instability onset has not been explored. In addition, no systematic investigation of the effect of the physical parameters has been done yet. Using a linear stability model, we investigate the effect of wave conditions, cross-shore profile, closure depth and two perturbation shapes (P1: cross-shore bathymetric profile shift; P2: bed level perturbation linearly decreasing offshore). For a P1 perturbation, no instability occurs below an absolute critical angle $\theta_{c0} \approx 40 - 50°$. For a P2 perturbation, there is no absolute critical angle: sandwaves can develop also for low-angle waves. In fact, the bathymetric perturbation shape plays a key-role in low-angle wave instability: such instability only develops if the curvature of the depth contours offshore the breaking zone is larger than the shoreline one. This can occur for the P2 perturbation, but not for P1. The analysis of bathymetric data suggests that both curvature configurations could exist in nature. For both perturbation types, large wave angle, small wave period and large closure depth strongly favour instability. The cross-shore profile has almost no effect with a P1 perturbation, whereas large surf zone slope and gently sloping shoreface strongly enhance instability under low-angle waves for a P2 perturbation. Finally, predictive statistical models are set up to identify sites prone to exhibit either a critical angle close to θ_{c0}, or low-angle wave instability.

1. Introduction

Sandy shorelines often exhibit alongshore undulations at different length scales. Well known examples are beach cusps (typical alongshore wavelength, $L \sim 1 - 50$ m) and megacusps (typically $L \sim 100 - 1000$ m), which are associated with swash zone processes and to surf zone rhythmic bars, respectively [*Ribas et al.*, 2015]. However, there are larger scale shoreline undulations with $L \sim 1 - 10$ km that are not directly linked to surf zone rhythmic bars but to similar undulations in the bathymetric contours up to a certain depth in the shoaling zone [*Ruessink and Jeuken*, 2002; *Davidson-Arnott and van Heyningen*, 2003; *Medellín et al.*, 2008; *Ryabchuk et al.*, 2011; *Kaergaard et al.*, 2012; *Idier and Falqués*, 2014]. We will call them kilometre-scale shoreline sandwaves or simply shoreline sandwaves. Some of these submarine geomorphic features can be forced by offshore bathymetric anomalies or by antecedent geological constraints [*Riggs et al.*, 1995; *Bender and Dean*, 2003; *Valvo et al.*, 2006]. Others, suspected to result from self-organisation processes, exhibit an alongshore migration. This migration is sometimes visually obvious (see e.g. *Davidson-Arnott and van Heyningen* [2003]; *Kaergaard et al.* [2012]), or is suggested by the observation of migrating zones of erosion and accretion (see e.g. *Ruessink and Jeuken* [2002]). Here, we focus on self-organized shoreline sandwaves.

The self-organized origin of coastal morphological patterns is widely accepted in case of beach cusps and rhythmic surf zone bars (see, e.g., *Coco and Murray* [2007] or *Ribas et al.* [2015]). In case of shoreline sandwaves, it has been hypothesized that they could emerge from a feedback between the morphology and the wave field involving: i) the wave driven longshore sediment transport and ii) the cross-shore sediment exchange between the surf and shoaling zones that is responsible for the cross-shore equilibrium profile. This feedback mechanism was proposed by *Ashton et al.* [2001] and later confirmed and refined in a number of modelling studies [*Falqués and Calvete*, 2005; *Ashton and Murray*, 2006a; *van den Berg et al.*, 2012; *Kaergaard and Fredsoe*, 2013a]. These studies show that sandwaves develop for (deep water) wave angle with respect to shore normal larger than a certain threshold, θ_c, with $\theta_c \geq \theta_{c0}$ and $\theta_{c0} \sim 42°$. In the present paper, θ_c will be called the critical wave angle and θ_{c0} the absolute critical wangle. However, *Idier et al.* [2011] found that for particular bathymetric profiles and wave conditions this positive feedback could also occur for low wave angles. These instabilities have been called High-Angle Wave Instability (HAWI) and Low-Angle Wave Instability (LAWI), respectively.

These modelling studies have extensively explored the basic instability mechanism, how it depends on the wave angle and its consequences on sandwave formation. Some of them have investigated the effect of wave height, wave period, bathymetric profile and closure depth on the growth rate (when there was instability) or wavelength of shoreline instabilities. For instance, after *Ashton and Murray* [2006b], an increase of wave height H and period T leads to an increase of the diffusional time scale ($\propto H^{12/5}T^{1/5}$), i.e. speeds up the sandwaves development in case of high-angle waves. *Kaergaard and Fredsoe* [2013a, b] investigated the effect of wave directional spreading, the closure depth D_c and the shoreface steepness and showed that sandwave wavelength increases with increasing directional spreading and D_c, while it decreases with increasing shoreface steepness. However, these studies did not investigate the effect of these parameters on the instability onset. *Falqués and Calvete* [2005] made a first investigation of the effect of wave conditions on this onset. They essentially found that instability develops only for large wave angle and is favoured by small H and small T. These authors explored the effect of 7 equilibrium profiles, showing that large slope at the shoreline and large bathymetric gradients on the shoreface favour instability onset. However, this exploration has been done for a limited number of bathymetric profiles and a single closure depth value was considered. *Idier et al.* [2011] made a systematic exploration of the effect of the wave height, the wave direction and the surf zone slope: they showed that small wave height and steep surf zones (e.g. a surf zone slope $\beta_s \geq 0.04$) could lead to instability onset for small angles. Thus, although previous modelling studies investigated the effect of wave conditions, bathymetric profile and closure depth, a systematic exploration of the instability onset for the whole range of realistic values of such parameters (with the same model) is lacking.

Another important issue is the bathymetric perturbation associated with the shoreline perturbation. It is indeed essential to capture the feedback between the morphology and the wave field. In morphodynamic models where the coastline evolves as a result of the changes in bathymetry driven by the sediment transport, both are linked in a natural way [*van den Berg et al.*, 2012]. However, in models based on the one-line concept, a link must be explicitly set up between shoreline and bathymetric perturbations. Both from observations and from physical principles, little is known on the perturbed bathymetry associated with self-organized sandwaves. Therefore, considering that sandwaves have a large time scale O($1-10$ yr) in comparison with the short term event scale of storms for instance, the assumption of a bathymetric perturbation corresponding to a cross-shore shift of the equilibrium profile following the shoreline displacement has been used (see e.g. [*Ashton et al.*, 2001; *Ashton and Murray*, 2006a]). Some studies (see e.g. [*Falqués and Calvete*, 2005; *Kaergaard and Fredsoe*, 2013a]) assumed this profile shift but by imposing a zero perturbation beyond the closure depth D_c. *Falqués and Calvete* [2005] considered other perturbations which are exponentially or linearly decreasing from a maximum value at the shoreline to 0 at D_c. Although some tests looking at different perturbation shapes have been done [*Falqués*, 2006; *Idier et al.*, 2011], there has been no systematic investigation of the effect of the various types of perturbation, and no analysis on the characteristics of the associated perturbed bathymetry, and especially on the bathymetric contour curvature, which, as we will show, plays a key role in the development of shoreline sandwave.

The present paper aims to systematically investigate the conditions which can lead to the emergence of km-scale shoreline sandwaves from instabilities driven by the alongshore sediment transport. The relative contribution of the physical parameters and the effect of the bathymetric perturbation shape on the instability onset are investigated, with a particular focus on the role of the bathymetric contour curvature and on the critical angle θ_c above which shoreline instability develops. First, the model is presented, the considered bathymetric perturbation shapes are introduced and their key properties are analysed, before describing the computer grid experiment (section 2). Then results are presented and the relative contributions of the physical parameters to the instability onset are analysed using statistical methods (section 3). Section 4 mainly discusses the sensitivity of the results to the considered perturbation shapes, the associated shoreline sandwave wavelengths, the shoreface slope effect, the plausibility of the perturbation shapes, and the probability to observe the absolute 42° critical angle in nature. Conclusions are drawn in section 5.

2. Model and methods

2.1. Model overview

The 1D-morfo linear stability model is used to investigate the conditions under which shoreline sandwaves can emerge from a morphodynamic instability. The model is fully described in *Falqués and Calvete* [2005] and only the main concepts are presented here along with some details on the shape of the assumed bathymetric perturbation (section 2.2).

A small undulation is imposed on an initially rectilinear shoreline being defined as:

$$y_s(x,t) = \frac{a}{2} e^{\sigma t + iKx} + c.c. \tag{1}$$

with x, y being cartesian coordinates in the alongshore and cross-shore directions (respectively), t the time, a the amplitude of the shoreline perturbation, K the alongshore wavenumber ($L = 2\pi/K$), $c.c.$ the complex conjugate and $\sigma = \sigma_r + i\sigma_i$ the complex growth rate (see Figure 1). The model aims at providing σ, from which the characteristic growth time σ_r^{-1} and the migration celerity $V = \sigma_i/K$ can be computed. A positive growth rate σ_r means that the shoreline perturbation of wavelength L develops.

Regarding the unperturbed state, the main inputs of the model are the cross-shore bathymetric profile, $z_b(y) = -D_0(y)$, and the significant wave height, peak period and angle at a certain depth: H_s (in meter), T_p (in second), θ (in degree). Regarding the perturbation, the main inputs are its alongshore wavelength, L, the depth of its offshore reach, D_c, and its cross-shore shape function, $f(y)$, so that $f(0) = 1$ and $f(y \geq y_c) = 0$, where $D_0(y_c) = D_c$. Thus, the perturbed bathymetry associated with the sandwave defined in Equation (1) is given by:

$$z_b(x,y,t) = -D_0(y) + \frac{a}{2}\beta_s f(y) e^{\sigma t + iKx} + c.c. \tag{2}$$

To compute the growth rate, σ, equation (1) is inserted into the one-line sediment conservation equation [*Komar*, 1998]:

$$\frac{\partial y_s}{\partial t} = -\frac{1}{\bar{D}}\frac{\partial Q}{\partial x} \tag{3}$$

where $\bar{D}$ is a mean depth of the morphodynamic active zone and Q is the total alongshore sediment transport rate. It should be noted that the one-line approximation presupposes that the response of the bathymetry to shoreline changes is instantaneous. Such assumption is justified only on time scale long enough for the sediment accumulation or deficit in the surf zone due to gradients in alongshore transport to be spread to the shoaling zone by the cross-shore exchange until the closure depth D_c. Such approach makes sense only in a long time scale, not in an event time scale, meaning that the model cannot describe the response to individual events such as storms. However, storms still play a significant role in the model behaviour as they affect the closure depth D_c, but in a statistical way [*Hallermeier*, 1978].

In Equation (3), Q is computed with the Coastal Engineering Research Center (CERC) formula [*Komar*, 1998]:

$$Q = \mu H_b^{5/2} \sin 2\alpha_b \tag{4}$$

where H_b, α_b are the wave height and wave angle with respect to the local shore normal at breaking and μ is an empirical constant. The constant μ (typical values of $\approx$ 0.1-0.2 $\mathrm{m}^{1/2}\mathrm{s}^{-1}$) is proportional to the empirical parameter K_1 of the original CERC formula. It is set up to $\mu = 0.15$ $\mathrm{m}^{1/2}$ s^{-1}, which corresponds to K1 = 0.525 (see [*Idier et al.*, 2011]). The value of μ has an effect only on the time scale, such that the sign of the growth rate σ_r (i.e. the shoreline instability onset) is insensitive to the magnitude of this parameter.

Computing the left hand side of equation (3) is straightforward from equation (1) but estimating the right hand side requires calculating the perturbed H_b and α_b. This is done by linearizing (with respect to a) the equations describing refraction and shoaling over the perturbed bathymetry and computing H_b and α_b numerically.

On many beaches, the long term averaged equilibrium profile can be represented by a Dean profile [*Dean*, 1977]. Thus, for the present analysis, we use a shifted Dean-type bathymetric profile, $D_0(y) = A((y+y_0)^{2/3} - y_0^{2/3})$, which is characterized by the A coefficient and the y_0 parameter that introduces a small shift to avoid an infinite slope at the shoreline [*Falqués and Calvete*, 2005]. We compute y_0 by prescribing the shoreline slope β_s, so that the bathymetric profile is fully defined by the two parameters A and β_s. Although β_s is (in the model) the slope right at the shoreline, its real meaning is the mean slope of the area where the littoral drift takes place (i.e. roughly the surf zone) since 1D-morfo is a one-line model so that this area collapses in a single line.

2.2. Bathymetric perturbation: description and role of the associated curvature

First, the cross-shore shape function (Equation 2) is such that $f(0) = 1$ and $f(y \geq y_c) = 0$ (see section 2.1). Second, as highlighted in the introduction, different types of bathymetric perturbation have been used in previous studies. The investigated perturbation shapes can be split in two classes : one based on profile shift assumptions, one based on a prescribed decay of the bed level perturbation. Two examples of bathymetric perturbations are provided in Figure 2, for low and high bathymetric gradients profiles.

The associated perturbation shapes can be written as follows:

$$P1 : f(y) = \frac{1}{\beta_s}\frac{dD_0}{dy} \tag{5}$$

$$P2 : f(y) = 1 - \frac{y}{y_c} \tag{6}$$

The shape function P1 (Equation 5) was defined and used by *Falqués and Calvete* [2005]. By inserting it in Equation (2) and considering Equation (1) it is readily seen that it corresponds to horizontally shifting the profile by the same amount as the shoreline displacement. The shape function P2 is based on a linear decay of the bed level perturbation (Equation 6). Such perturbation is obtained as a limit of the exponential perturbation used in [*Falqués and Calvete*, 2005] in case of very large value of the e-folding distance controlling the seaward decay, i.e. the distance over which the bed level perturbation decays by a factor $\exp(1) \simeq 2.7$.

For the high bathymetric gradient, both options show similar (but not exactly equal) horizontal patterns (Figure 2b), whereas for the low bathymetric gradient, P2 exhibits significant differences with a curvature of the bathymetric lines which reaches a maximum at a certain distance from the coast (Figure 2a).

We here make a preliminary analysis of this curvature property on shoreline sandwave development. First, wave refraction by slowly varying depth contours can be represented by wave rays, which are locally perpendicular to the wave fronts [*Mei*, 1989]. In case of curvilinear depth contours, the bathymetry can be locally approximated by circular contours. Then, the following generalized Snell law $kr\sin\theta = C_0$ is valid, where C_0 is a constant, k is the wavenumber, r is the distance to the center of curvature and θ is the angle between wave rays and the local normal to the contours [*Mei*, 1989]. Then, if $\theta \neq 0$

in deep water, it can never be 0 in shallower water and, as a result, wave rays approaching with certain angle can never cross the normal to the bathymetric lines.

One of the main differences between the work of *Idier et al.* [2011] and other shoreline sandwave studies is the existence (or not) of a critical angle, or in other words, if LAWI is active or not. Therefore, it is useful to focus on the case of offshore waves characterised by an incidence angle normal to the coast ($\theta = 0°$). In this case the growth of a bump in the shoreline needs a sediment flux, Q, directed towards the tip at both sides of the bump. If the depth contours are parallel to the shoreline (P1), this means that the wave rays should cross the normal to the depth contours, which is impossible according to the generalized Snell law. Therefore, LAWI can never occur if a P1 perturbation is assumed.

The situation is different in case of a P2 perturbation, because the depth contours are no longer parallel to the shoreline and their undulations could in fact be more pronounced than the shoreline undulation (see Figure 2a). If this is the case, the rays can cross the normal to the shoreline without crossing the local normal to the depth contours during refraction. In this case the sediment fluxes converge at the tip so that LAWI could occur. To examine this possibility, we compute the maximum angle (ϕ) between a perturbed bathymetric contour and the mean shoreline. By linearising with respect to a the real part of Equation (2) for $t = 0$, this angle is given by:

$$tan\phi = a\beta_s K \frac{f(y)}{D_0'(y)} \quad (7)$$

By inserting the Dean type profile $D_0(y)$ and the P2 shape function $f(y)$ one obtains:

$$tan\phi = \frac{3a}{2} \frac{\beta_s K}{A y_c} F(y) \quad (8)$$

where $F(y) = (y_c - y)(y + y_0)^{1/3}$. This function has a maximum at $y_m = (y_c - 3y_0)/4$. If $y_m > 0$ there is a region between the shoreline, $y = 0$, and a certain offshore location y_1 ($> y_m$), where the curvature of the depth contours is larger than the curvature of the shoreline. By using Equation (27) of *Falqués and Calvete* [2005] that gives y_0 as a function of A and β_s and after some algebra, one obtains the location y_m of maximum bathymetric curvature :

$$y_m = \frac{1}{4}\left(\frac{D_c}{A}\right)^{3/2}\left((1+\frac{4}{9}\Omega)^{3/2} - \frac{32}{27}\Omega^{3/2}\right) \tag{9}$$

where, $\Omega = A^3/D_c\beta_s^2$ is a dimensionless parameter. It can be seen that $y_m > 0$ for:

$$\Omega = \frac{A^3}{D_c\beta_s^2} < \frac{9}{4 - 2^{10/3}} \simeq 1.48 \tag{10}$$

Thus, Equation (10) provides a necessary condition for having LAWI in case of a P2 perturbation and shows that LAWI should be favoured by small A, large D_c and large β_s. Such result is consistent with the conclusion of *Idier et al.* [2011] who found that instabilities can develop in cases of low-angle or shore normal incidence under the condition of large enough beach slope and large enough cross-shore extension of the bed perturbation (i.e. large enough closure depth in the case of a P2 perturbation). As soon as $\Omega \geq 1.48$, y_m is located at the shoreline, as for the P1 perturbation. Figure 2 illustrates the effect of an increase of A (i.e. Ω) on the bathymetric undulations. For the small A value ($\Omega = 0.043$, panel a), bathymetric undulations are maximum at a certain distance from the coast, while for large A ($\Omega = 0.86$, panel b), they reach a maximum closer to the shoreline such that the P2 bathymetric contours are quite similar to the P1 ones. This analytical development suggests that we should observe similar results (e.g. similar critical wave angle θ_c) between the P1 and P2 perturbations for large A and small β_s. As soon as $\Omega \geq 1.48$, only HAWI can develop in the case of a P2 perturbation. To illustrate the physical conditions corresponding to the critical value $\Omega = 1.48$, assuming physical ranges for D_c and A, we compute the slope $\beta_s(\Omega = 1.48)$ (Figure 3). For given A and D_c values, if β_s is smaller than $\beta_s(\Omega = 1.48)$, then there is no possibility to observe low-angle instability (as y_m is located at the shoreline).

The Ω condition is necessary but not sufficient to trigger LAWI: another necessary condition is that $y_1 > y_b$ (y_b is the position of the unperturbed breaking line), i.e., the region where the curvature of the depth contours is larger than the curvature of the shoreline extends offshore the surf zone such that the refractive bending of the rays before breaking can be stronger than the rotation of the shoreline. This second necessary condition of a narrow (enough) breaking zone depends on both the wave conditions and the A coefficient. The above analysis suggests that the conditions prone to sandwave formation for any wave angle (i.e. also for low angles) are large β_s, small A and large D_c (i.e. small Ω), but also small wave period and wave height.

2.3. Computer experiment set-up

To confirm this analysis and investigate the effect of the physical and model parameters on the instability onset, a systematic analysis is done by performing a model grid experiment in the space $(\theta, \beta_s, A, D_c, H_s, T_p)$. A wide range of physically possible parameter values on sandy coasts is explored (Table 1).

For each configuration $(\theta, \beta_s, A, D_c, H_s, T_p)$ we computed the growth rate with the 1D-morfo model for shoreline perturbations of wavelengths L ranging from 10 m to 50 km, with a step of 100 m (i.e. for 500 different wavelengths). The shoreline is considered unstable when at least one perturbation within the wavelength range is amplified (i.e. $\max(\sigma_r(L)) > 0$). A large enough wavelength range is considered in order to ensure capturing the unstable wavelengths at their initiation stage. It should be noted that this study focuses on the conditions leading to shoreline instability, rather than on characteristics of the linearly most amplified modes such as the wavelength (for further information on these characteristics, see for instance the study of *Idier et al.* [2011] which covers the entire range of wave incidence angle, but for a limited number of configurations, and section 4.2 for a statistical analysis of the wavelengths of the linearly most amplified modes obtained from the grid experiment).

The range of the parameters H_s and T_p are representative of yearly averaged wave conditions encountered along the world coasts. They are estimated using global wave model results analysis. The wave data come from a global wave hindcast done using the CFSR wind data and the WW3 model (spatial resolution of 0.5°, temporal resolution of 3 h), within the IOWAGA project [*Rascle and Ardhuin*, 2013]. This wave hindcast is also used, to estimate the range of possible D_c values on a decade scale by using the Hallermeier formula [*Hallermeier*, 1981]. The values of A and β_s are selected based on existing literature and physical considerations. We choose a maximum value of $A = 0.3$ m$^{1/3}$ based on the *Dean* [1987] relationship between the fall velocity and A, which for coarse sand of 2 mm gives $A = 0.25$ m$^{1/3}$. As a comparison, existing shoreline sandwave studies using a Dean profile [*Falqués and Calvete*, 2005; *Kaergaard and Fredsoe*, 2013a, b; *Uguccioni et al.*, 2006; *van den Berg et al.*, 2012; *Idier et al.*, 2011] considered A coefficients falling in the range $0.08 - 0.2$ m$^{1/3}$. For the maximum value of β_s, a value of 0.2 would be justified according to the literature (e.g., *Wright and Short* [1984]). However, to account for the inherent degree of uncertainty and some possible extremely steep surf zones, we extend the β_s range to 0.5. In addition, to ensure considering physical values, three constraints have been taken into account in the computer grid experiment design: (C1) the critical wave steepness, (C2) the consistency between surf zone slope and shoreface shape, (C3) the closure depth versus the wave conditions. Indeed, waves are characterized in nature by a maximum steepness, such that the wave period T_p cannot be smaller than a given value for a given wave height H_s. The *Pierson and Moskowitz* [1964] criteria is used to estimate the minimum wave period versus the wave height (constraint C1). Regarding the bathymetric profile, the mean surf zone slope β_s cannot be smaller than the mean shoreface slope D_c/y_c (constraint C2, see Figure 1). This leads to the constraint that the minimum value of β_s depends on A and on D_c . Finally, the closure depth D_c (obtained considering the wave conditions corresponding to the 12 hours exceeding wave height over a given time span, see [*Hallermeier*, 1981]), by definition, cannot be smaller than the closure depth that we would obtain using mean wave climate conditions (constraint C3). These constraints imply that the grid experiment is not uniform, i.e. the number of simulations per bin is not constant (as shown by the non-uniform colors in each panel of Figure 4). For instance, focusing on the distributions of the computations versus the slope β_s (Figure 4, left panel), the number of simulations per bin (n_b) is not constant (n_b is constant for $\beta_s \geq 0.04$ but not for smaller β_s values). This is due to the C2 constraint. The grid experiment dataset represents 1 004 652 (i.e. about 1 million) simulations per bathymetric perturbation type. Each run costs 1.2 s of computation on one CPU (Central Processing Unit), such that the computational effort, in CPU unit, represents 14 days for each perturbation type. The computations have been done on 40 CPU's.

3. Results

3.1. General trends

For each configuration $(\beta_s, A, D_c, H_s, T_p, \theta)$, the model provides the maximum growth rate $(\max(\sigma_r(L)))$ for the explored range of wavelength (10 m − 50 km), i.e. a single deterministic value. If this value is positive, then there is instability (shoreline sandwaves develop).

Analysing results in the 6 dimensions space of the input parameters $(\beta_s, A, D_c, H_s, T_p, \theta)$ raises the issue of the visualisation for high dimension problems. To tackle this issue, we analyse the results in terms of probability of shoreline sandwave development in 2 dimensions spaces. This is done by defining the probability $p_s(\theta, X_i)$ (with $i = 1$ to 5 and $X = (\beta_s, A, D_c, H_s, T_p))$ as the ratio of the number of experiments for which instability develops for a given bin (θ, X_i) to the total number of experiments done in this bin. For instance, the probability $p_s(\theta = 85°, D_c = 25\text{ m})$ is equal to the number of cases where instability develops in the space $(\beta_s, A, D_c = 25\text{ m}, H_s, T_p, \theta = 85°)$ divided by the total number of runs done in this space (see Figure 5a3).

As highlighted in section 2.3, the grid experiment is not uniform (Figure 4). To better highlight the general trend avoiding side effect due to the non-uniformity, in addition to the "all grid" dataset, we consider two uniform subsets. Both subsets include the entire range of wave angle and shoreface slope, but exclude the surf zone slopes smaller than 0.04. Subset 1 includes the entire range of wave height H_s but includes only the largest values of D_c ([10-27.5] m) and T_p ([8-16] s), while Subset 2 includes the entire range of D_c and T_p but includes only the lowest wave height values ([0.25-1]m).

Figure 5 shows the probability of shoreline sandwave development $p_s(\theta, X_i)$ for the P1 and P2 perturbations. First, although the perturbation shapes P1 (profile shift) and P2 (linear bed level decay) may be relatively similar in some cases (see e.g. Figure 2b), the probability patterns strongly differ when comparing the a) and b) panels of Figure 5. The most crucial difference is that for P1, there is an (absolute) critical angle θ_{c0} ($\sim 42.5° \pm 2.5°$), below which $p_s = 0$ whatever the physical parameters, whereas for P2, even though p_s increases with the angle, there is no critical angle. 33% of the runs done over the entire space $(\theta, \beta_s, A, D_c, H_s, T_p)$ exhibit the same results (instability/stability) for both perturbation shapes, i.e. $\max(\sigma_r(L)) > 0$ or $\max(\sigma_r(L)) \leq 0$.

In addition to the effect of the perturbation shape, Figure 5 allows analysing the dependency of the instability onset on the physical parameters. To avoid misinterpretation of the results, we now consider the p_s values obtained for the uniform subsets 1 and 2. Focusing on perturbation shape P1 in areas of potential instability (i.e. where $p_s > 0$), the probabilities are overall smaller than for the P2 shape (Figure 5a and b). The probability tends to 1 only for oblique waves characterised by small wave periods, meaning that in such case, there would be instability whatever the values of the other parameters. The probability p_s increases with D_c, while there is a slight influence of A and no influence of the surf zone slope β_s and wave height H_s. Figure 5 suggests the following ranking (from dominant to minor) of the parameters contributions: θ and T_p, D_c, A. The null effect of β_s can be readily seen by replacing the P1 perturbation shape function $f(y)$ provided by Equation (5) in the model Equation (2), as β_s cancels in this case.

Regarding the P2 perturbation, β_s and A have a positive and negative effect, respectively (Figure 5b-1,2). Thus the two parameters characterizing the bathymetric profile play opposite roles. Indeed, small A values lead to stronger wave refraction, whereas large surf zone slope β_s leads to a smaller surf zone width. According to *Idier et al.* [2011] who assumed perturbations similar to the P2 type, large refraction and small surf zone width favour shoreline sandwave development, especially for low incidence angle. The negative effect of A for the P2 perturbation will be further discussed in section 4.3. Regarding the closure depth D_c, it has a positive effect (Figure 5b-3), while the wave period T_p and height H_s have a negative effect on shoreline instability development (Figure 5b-4,5). In terms of relative influence of the parameters, the variations of probability induced by each parameter suggest that β_s, θ, A and D_c have significant effects while H_s and T_p have minor effects on the instability onset. These results overall confirm the findings of previous work. For example, *Falqués and Calvete* [2005] found, for the same perturbation type, that increasing the wave steepness or decreasing wave height tend to strengthen instability. *Idier et al.* [2011] showed that increasing β_s or D_c favour instability. Both papers provided an explanation of the related physical mechanisms. But what was not clearly identified before is the relative effect of the bathymetric profile (β_s and A) and the relative contribution of the other parameters.

The negative (A) and positive effects (β_s and D_c) drawn form the numerical computations are consistent with the preliminary analysis done in section 2.2 which highlights the necessary condition for instability in case of normal wave incidence $\Omega = A^3/D_c\beta_s^2 < 1.48$ (i.e. a curvature of the bathymetric contours larger than the one at the shoreline). In addition, the analysis of the grid experiment results shows that the Ω values of the unstable configurations range between 0 and 0.3, and that the critical value of Ω below which instability occur also depends on D_c, H_s, T_p (see Figure S.1 in Supplementary Material). This is consistent with our conclusion of section 2.2: instability should be triggered only when the bathymetric curvature offshore the breaking line is larger than the shoreline one (i.e. under the necessary condition that Ω is smaller than 1.48 and a narrow enough breaking zone). Considering the entire range of wave direction, only 32 configurations over the 829921 instability cases exhibit an Ω value larger than 1.48. These 32 configurations exhibit a wave incidence angle $\theta \geq 60°$.

To summarize, the perturbation shape and the related bathymetric curvature play a key role, while instability onset is favoured by large wave incidence (θ), large closure depth (D_c) and small wave period (T_p), whatever the perturbation type.

3.2. Relative influence of the parameters versus wave angle

The effect of the physical parameters depends on the wave angle (as shown in Figure 5). To better assess this dependence, we compute the ratio $R_{X_i}(\theta) = (p_s(\theta, \max(X_i)) + 1)/(p_s(\theta, \min(X_i)) + 1)$, for each parameter X_i, with $X = (\beta_s, A, D_c, H_s, T_p)$. $R_{X_i}(\theta) > 1$ ($R_{X_i}(\theta) < 1$) means that, for a given wave angle, an increase of X_i leads to an increase (decrease) of the probability of shoreline sandwave development. $R_{X_i}(\theta) = 1$ means that for this θ value the X_i parameter has no effect. A constant $R_{X_i}(\theta)$ means that the effect of the parameter X_i is independent of θ. Thus if $R_{X_i}(\theta)$ goes close to 1 for increasing θ, this means that the effect of the parameter X_i is decreasing with θ. $R_{X_i}(\theta)$ is computed for the entire grid experiment (set called "all grid") but also for subsets 1 and 2.

First, we focus on the results obtained with a P2-type perturbation for subset 1. In agreement with the results of section 3.1 (Figure 5b-S1), β_s and A have the largest effects (positive for β_s, negative for A) while D_c, H_s and T_p have smaller effects (Figure 6b, bottom panel). H_s has a negative effect whose amplitude decreases with θ. In addition, the effects of the cross-shore profile (β_s and A) and the closure depth D_c are enhanced by low wave angles. Finally, the amplitude of the contribution of T_p increases with increasing wave angle until $\theta = 60°$ and then decreases, whereas the amplitude of the other contributions mainly decreases with the wave angle. In terms of relative contribution, it should be reminded that the above analysis is done for subset 1 where the smallest values of D_c and T_p of the grid experiment are not included (see section 3.1). Selecting the subset 2, which includes these small values but excludes the large values of H_s, leads to similar curves, but with larger R_{D_c} values and larger variations of R_{D_c} with θ. These results are confirmed when taking into account the entire grid experiment (Figure 6b, top panel): in case of a P2 perturbation, the dominant parameters appear to be β_s, A and D_c.

The P1 perturbation exhibits a different behaviour (Figure 6a, top panel). First, consistently with the existence of an absolute critical angle $40° < \theta_{c0} < 45°$ observed in section 3.1, $R_{X_i} = 1$ until $\theta = 40°$. Focusing on subsets 1 and 2, Figure 6a (bottom panel) also shows that: A has a positive effect (contrary to P2) which increases with θ; D_c has a significant positive effect (as P2) mainly increasing with θ (contrary to P2); T_p has a significant negative effect (as P2), whose amplitude increases with θ (as P2 for $\theta \leq 60°$); β_s and H_s have no effect (contrary to P2). The more striking difference with the case of a P2 perturbation is the positive effect of A. This will be discussed in section 4.3.

3.3. Critical wave angles θ_c and θ_{c0}

The variations of the $p_s = 0$ contours with the parameters X_i (see e.g. subsets 1 and 2 on Figure 5) indicate that for a P1 perturbation, changes in β_s and H_s do not affect the critical angle θ_c, while the increase of D_c, of T_p, and to a smaller extent of A, leads to a decrease of θ_c. For the P2 perturbation, the changes in p_s indicate that θ_c decreases with β_s and D_c, while it increases with A and H_s, and hardly changes with T_p.

As highlighted above, in the P1 case, whatever the parameters $(\beta_s, A, D_c, H_s, T_p)$, there is an absolute critical wave angle over the entire experiment (θ_{c0}) of $42.5° \pm 2.5°$. Then, what are the conditions prone for exhibiting a critical angle equal to the absolute one ($\theta_c = \theta_{c0}$) in case of a P1 perturbation? Contrary to the P1 case, in the P2 case, there is no absolute critical angle and shoreline sandwaves can develop for low-angles under certain conditions. Then, what are the conditions prone for exhibiting no critical angle (i.e. that instability develops for $\theta = 0°$) in case of P2 perturbation?

To tackle these questions and quantify the relative importance of the parameters X_i, first, we compute the critical angle θ_c for every combination $(\beta_s, A, D_c, H_s, T_p)$ (for an example, see Figure S.2 in Supplementary Material). Cases where the critical wave angles are strictly equal for perturbations P1 and P2 represents about 8.32% of the experiment, in the space $(\beta_s, A, D_c, H_s, T_p)$. Then, we use a logistic regression method (see *Hothorn and Everitt* [2014], Chapter 7), focusing on the probability p that $\theta_c = \theta_{c0}$ in the P1 case, and that θ_c does not exist in the P2 case. The Logit function is defined as $\text{Logit}(p) = \log(p/(1-p)) = \log(\text{odds ratio})$ and $\text{Logit}(p)$ is approximated by a linear combination of the parameters, i.e. in the present case $(\beta_s, A, D_c, H_s, T_p)$, such that:

$$\text{Logit}(p) = a_0 + a_{\beta_s}\beta_s + a_A A + a_{D_c} D_c + a_{H_s} H_s + a_{T_p} T_p \tag{11}$$

The obtained logistic regression model exhibits a good fit with the data ($R^2 \sim 89\%$ and $\sim 75\%$, for the P1 and P2 perturbations, respectively) and a good prediction skill (with an area under the ROC curve of 99.6% and 96.3%, respectively ; see *Metz* [1978] for details on the ROC analysis principle).

First, the logistic regression coefficients (Table 2) show that $p(\theta_c = \theta_{c0}, X)$ only depends on A, D_c and T_p in case of a P1 perturbation (consistently with the results of the previous subsections). Figure 7a shows, in the space (A, D_c, T_p), the restricted number (8% of the explored combinations $(\beta_s, A, D_c, H_s, T_p)$) of cases where $\theta_c = \theta_{c0}$. In case of a P2 perturbation, the regression coefficients (Table 2) show that $p(\theta_c$ does not exist, $X)$ only depends on β_s, A, D_c and H_s (indeed T_p has a non significant effect as indicated by the high p-value of the Wald statistics). The distribution of the configurations of the grid experiment leading to the non existence of θ_{c0} in the space (β_s, A, D_c, H_s) shows that the number of such configurations is high (Figure 7b, in black) .

Second, the sign of the coefficients (Table 2) indicate that, for P1, A and D_c increase the odds ratio for observing the absolute critical angle θ_{c0}, while T_p decreases it. For P2, β_s and D_c increase the odds ratio for not observing any critical angle θ_c, whereas A and H_s decrease these odds, consistently with the results of section 3.2.

Third, one interest of the statistical analysis is that the obtained normalized coefficients (Table 2) allow to rank the effect of the parameters. In case of the P1 perturbation, the relative effect of T_p is larger than the one of D_c, which is much larger than the one of A. From the largest to the smallest, we can also rank the parameters for the case of a P2 perturbation: β_s, A, D_c, H_s. However, this should not be interpreted as an absolute result as it is sensitive to the range of X_i (Table 1). The dimensional coefficients can be used to compute the dimensionless ones when different parameters ranges are considered, and thus to rank the contributions for the considered ranges.

Finally, this logistic approach allows to estimate the probability p, using the relationship $p = 1/(1 + e^{-\mathrm{Logit}(p)})$ and Equation 11 to compute Logit(p). Then, in a given site, if the parameters (i.e. the vector X) are known, the probability p can be estimated using the dimensional regression coefficients, and thus without requiring any additional model run (see section 4.5 for an example).

For instance, for a P1 perturbation, considering different ranges for β_s ([0.02,...,0.1] or [0.02,...,0.2]), A ([0.05,...,0.1] or [0.05,...,0.2] m$^{1/3}$), D_c ([5,...,10] or [5,...,20] m) and assuming $H_s \in$ [0.5,...,3] m and $T_p \in$ [5,...,15] s, we find that $p(\theta_c = \theta_{c0})$ is most of the time equal to 0, confirming the low probability to observe $\theta_c = \theta_{c0}$. Equation (11) can also be used to identify the sites prone to $\theta_c = \theta_{c0}$ by estimating one of the three significant parameters (e.g. D_c) as a function of the two others (e.g. A and T_p) for a given value of the probability p :

$$D_c = c_0 + c_p \text{Logit}(p(\theta_c = \theta_{c0})) + c_{T_p} T_p + c_A A \tag{12}$$

with $c_0 = -a_0/a_{D_c}$, $c_p = -1/a_{D_c}$, $c_{T_p} = -a_{T_p}/a_{D_c}$, $c_A = -a_A/a_{D_c}$, such that $c_0 = -15.848$ m, $c_p = 1.695$ m, $c_{T_p} = 6.085$ m/s and $c_A = -24.407$ m$^{2/3}$. A is one to two orders of magnitude smaller than T_p while c_{T_p} and c_A have similar order of magnitude. This illustrates the minor effect of A, compared to T_p, as shown in Table 2. Equation (12) is used to identify the combinations prone to exhibit the absolute critical angle, for instance with a probability $p(\theta_c = \theta_{c0}) = 0.95$ (Figure 8). Taking into account that large closure depths are not expected to be much larger than about 30 m, sites where the absolute critical angle is likely to be observed should be characterised by wave period smaller than 7-8 s (as shown in Figure 8), and even smaller (e.g. $\sim$ 4 s) when considering smaller closure depths (e.g. $\sim$ 10 m). Thus, if we assume that in nature, perturbations could be of type P1, there should be a low probability to observe the absolute critical angle θ_{c0} and the sites prone to exhibit it would be those characterised by a small wave period and/or a large closure depth. Using Equation (12) with a large p value could help identifying such sites, and thus, if $\theta \geq \theta_{c0}$, sites prone to HAWI.

In the case of P2 perturbation, considering the same parameters ranges as in the previous paragraph, the probability p that there is no critical angle appears to be quite large, almost never equal to zero. Depending on the considered ranges, each of the parameters H_s, D_c, A or β_s may be the dominant parameter. If we assume that in nature, perturbations could be of type P2, then there should be a strong probability to observe shoreline sandwaves.

4. Discussion

4.1. Sensitivity to the bathymetric perturbation

The instability onset has been investigated for two bathymetric perturbation shapes. The sensitivity of the results to this choice is investigated considering the following additional perturbation shapes:

$$P3: f(y) = \frac{1}{\beta_s}\frac{dD_0}{dy}\left(1-\frac{D_0}{D_c}\right) \tag{13}$$

$$P4: f(y) = 1 \text{ if } y \leq y_b,\ f(y) = 1-\frac{y-y_b}{y_c-y_b} \text{ otherwhise} \tag{14}$$

First, as stated in [*Falqués and Calvete*, 2005], strictly speaking, the profile shift perturbation P1 is incompatible with the concept of closure depth since in this case there is a bathymetric perturbation which decays offshore but which extends up to infinity, i.e., beyond the closure depth. As a consequence, the profile shift perturbation has the drawback to present a discontinuity at y_c. Even if the jump in bed level at D_c is small, the depth contours are all parallel to the undulating shoreline until D_c and then suddenly straight, which is unrealistic. To address these drawbacks, a second shape function (P3) is considered, characterised by a gradual decrease in the perturbation of the depth contours to straight lines at D_c (Equation 13). Second, the 1D-morfo model does not resolve the surf zone, which, in one-line models, collapses into the "shoreline". For this reason, a perturbation that starts to decay already in the surf zone seems questionable. Following this idea, a fourth shape function (P4) is defined such that P4 is equal to 1 in the surf zone and decreases linearly from 1 at the breaking point to 0 at $D = D_c$ (Equation 14), as in [*Idier et al.*, 2011].

The probability of instability onset (p_s) obtained with the P3 and P4 perturbations (Figure S.3 in Supplementary Material) exhibits similar patterns as those obtained with the P1 and P2 perturbations, respectively: in case of a P3 perturbation, an absolute critical angle $\theta_{c0} = 47.5° \pm 2.5°$ is found, whereas for a P4 perturbation, instability cases occur for the entire range of θ values. This suggests that there are two types of bathymetric perturbations: those where the curvature of the bathymetric contours is always smaller than (or equal to) the shoreline curvature (P1,P3) and those where the curvature can be larger than the shoreline curvature (P2,P4). The first type leads to the existence of an absolute critical angle θ_{c0}, while the second type leads to the absence of such absolute critical angle. However, P3 leads to much smaller probabilities (2 to 3 times smaller) than P1 but also to a smaller range of parameters leading to instability. Regarding P4, the quantitative results are quite close to the ones obtained considering a P2 perturbation: the areas of instability are the same and the probabilities are only slightly larger, with differences smaller than 10 %.

4.2. Shoreline sandwave wavelength

The modeling results highlight the key role of the bathymetric perturbation shape on the instability onset. In addition to this information, the 1D-morfo model provides the wavelength of the Linearly Most Amplified mode (LMA) for each investigated configuration (see section 2.3). For both perturbation shapes P1 and P2, the LMA modes exhibit wavelengths ranging from few hundred meters to several tens of kilometres (Figure 9), i.e. correspond to km-scale shoreline sandwaves. The main difference is that for a P1 perturbation the quartiles of the wavelengths of the grid experiment decrease with the wave incidence angle, while for a P2 perturbation these statistical moments first increase (until $\theta \simeq 50°$) and then decrease with θ. In addition, the overall LMA wavelengths are larger for a P1 perturbation, while for very oblique waves ($\theta \geq 70°$), the wavelengths are of the same order of magnitude (1 ± 0.5 km) for both perturbation shapes. Thus, the bathymetric perturbation shape plays a key role not only on the instability onset, but also on the wavelength of the associated Linearly Most Amplified mode.

4.3. Shoreface slope effect

As shown in section 3.1, the overall shoreface slope, characterized by A, has a positive effect on the instability in case of P1 and negative in case of P2. The reasons for this can be investigated by looking at the expression of the complex growth rate provided by *Idier et al.* [2011], equation (7). By examining the e_2 and the e_3 terms, related to the perturbation in wave angle and in wave height, respectively, it turns out that only $e_2 = 2\theta'_{bi}/Ka$, where θ'_{bi} is the imaginary part of the perturbed wave angle at breaking, exhibits opposite trends when increasing A (we here adapted the expression to the notation and the definition of the amplitude, $a/2$, in the present paper). It increases (decreases) with A in case of a P1 (P2) perturbation. This term is related to refraction and is always positive as a result of wave rays tending to rotate in the same direction as the bathymetric contours. Thus, for both perturbation shapes, the behaviour with respect to A is related to wave refraction.

The influence of A and of the shape of the bathymetric perturbation on wave refraction (here on the θ_i' variable) can be understood by focusing on normal wave incidence and looking at equation (A3) in [*Falqués and Calvete*, 2005]. Taking the water depth, $D = D_0(y)$, as independent variable, this equation can be cast into:

$$\frac{d}{dD}(k_0(D)\theta_i'(D)) = -K\,\frac{\Phi(D)}{\beta(D)}\,\hat{h}(D) \tag{15}$$

where $\beta(D) = dD_0(y)/dy$, $k_0(D)$ is the wavenumber of the water waves, $\Phi(D)$ collects various functions of D defined from linear water wave theory and $\hat{h}(D) = a\beta_s f(D)/2$. Notice that this equation is linear, with homogeneous boundary condition, $\theta_i'(D_c) = 0$. Therefore, if the forcing term is multiplied by a constant, the solution $\theta_i'(D)$ will be the same but multiplied by this constant.

In case of a P2 perturbation, $\hat{h}(D)$ does not depend on A since it cancels out from the ratio y/y_c in Equation (6). On the other hand, $\beta(D)$ is proportional to $A^{3/2}$ for each D. Then, the dependence on A is only present in the forcing term through $\beta(D)$ and therefore, the solution $\theta_i'(D)$ decreases by increasing A, and so will do $\theta_{bi}'(D) = \theta_i'(D_b)$. Therefore, the instability is favoured by decreasing A.

In case of a P1 perturbation, $\hat{h}(D) = a\beta(D)/2$, so that the forcing term does not depend on A with the result that $\theta_{bi}'(D)$ does not depend on A either. Thus, the instability should be insensitive to A. In the case of oblique wave incidence, another term appears in Equation (A3) of [*Falqués and Calvete*, 2005]. The analysis in this case is not simple but it turns out that the additional term makes $\theta_{bi}'(D)$ to increase with A, i.e. that instability is favoured by large A.

4.4. Bed perturbation in nature?

To find out whether these types of perturbation shape do represent sandwave bathymetry, we should analyse bathymetric data in coastal areas exhibiting shoreline sandwaves. However, we face two difficulties: (1) detailed observations of self-organized sandwaves are scarce and this is even worse regarding the bathymetry associated with the sandwaves, (2) when sandwaves are observable they can hardly be considered in the early stage of formation for Linear Stability Analysis to be applicable. As a first attempt to characterise the curvature of perturbation shape from real cases in nature, we analyse three shoreline sandwave sites where processed bathymetric data are available (Figure 10): Holmslands Tange [*Kaergaard et al.*, 2012], the distal end and tow of the Long Point spit of Lake Erie [*Davidson-Arnott and van Heyningen*, 2003].

The Holmslands Tange site is characterised by sandwaves of small amplitude ($a/L = 0.008$, with $L = 5$ km). We use the filtered isobathymetric lines digitized from [*Kaergaard et al.*, 2012] (Figure 12 herein, where the bars have been removed). The depth contours stop at 5 m depth (Figure 10a). However, *Kaergaard et al.* [2012] and *Falqués et al.* [2017] suggest that D_c would be substantially larger than 5 m.

The Long Point sandwaves are characterised by larger relative amplitudes ($a/L = 0.1$, with $L \sim 1$ km, after *Davidson-Arnott and van Heyningen* [2003]). We use the bathymetric contours provided by NOAA (data available at http://www.ngdc.noaa.gov/mgg/greatlakes/erie.html)(Figure 10b,c). These contours do not include the shoreline $D = 0$ m. Thus, the analysis focuses on the depth contours $D = 1$ m to $D = D_c$, with $D_c \sim 11$ m (see section 4.5 for the estimation of D_c).

To avoid any effect of small features (e.g. sandbars) or larger features (e.g. the spit related curvature), small and large wavelengths are filtered out from the bathymetric contours (for Holmslands Tange, $L < 200$ m and $L > 7000$ m are filtered out ; for the Long Point site, $L < 200$ m and $L > 2000$ m are filtered out). Then, we compute $C(D, x) = |dy/dx|$ along each depth contour. As the depth contours are undulating, for a given wavelength, the mean ($\bar{C}(D)$) of $C(D, x)$ and the linear regression prediction $\hat{C}(D)$ (obtained by minimising the least mean square error over the entire dataset) can be considered as indicators of the maximum curvature associated with a water depth D. Both indicators are increasing (decreasing) in the offshore direction for Holmslands Tange (Long Point sites) (Figure 10).

Thus, the observed bathymetry at Holmslands Tange supports the essential curvature characteristics of a perturbation of type P2, i.e., a maximum curvature of the bathymetric lines away from the shoreline. This suggests that the type of bathymetric perturbation observed on this site is prone to instability even for wave incidence angles smaller than $\simeq 42°$. At Long Point, the observed bathymetry would support the curvature characteristics of the P1 or P3 type, suggesting that this site is not prone to LAWI but prone to the existence of an absolute critical angle. This is one reason for observing $\theta_c \simeq 42°$ on this site (as in [*Ashton and Murray*, 2006b]).

In this analysis, we assumed that: (1) in the chosen wavelength range (e.g. 200 m to 2000 m for the Long Point sites), all the dominant bedforms are related to sandwaves, (2) the shoreline sandwaves have a small enough amplitude for assuming that sandwaves are at their initiation stage (this could be the case for Holmslands with $a/L = 0.008$, while this is not the case at Long Point spit with $a/L \sim 0.1$). Both assumptions are debatable. However, it is still remarkable to observe that both cases could happen in shoreline sandwaves area: increase or decrease of depth contour curvature in the offshore direction. Further systematic investigations on other sandwave sites are necessary to confirm this preliminary analysis, but they require detailed bathymetric data which are still lacking in such areas.

As a preliminary analysis, it seems that several factors could favour bathymetric anomalies supporting the essential curvature characteristics of a perturbation of type P2. First, it is worthwhile to notice that offshore tidal and current sandwaves have been observed off the Holmsland coast, at depths ranging from 8 to 18 m [*Anthony and Leth* , 2002]. Second, after the study of *Limber et al.* [2017] on the Rodanthe shoreline (USA), shoals could trigger the development of shoreline sandwave under waves of low incidence angle. On the Rodanthe site, as a consequence of the shoal, the depth contours reach a maximum curvature larger than the one of the shoreline. This effect of shoal on shoreline sandwave developement under low incidence angle is consistent with the theoretical work of *Idier et al.* [2011]. Thus, there are indications that offshore morphodynamic and/or geological features could favour perturbations of type P2. However, further investigations are required to better understand which conditions favour which perturbation.

4.5. Critical Angle for HAWI

All modeling studies [*Ashton et al.*, 2001; *Falqués and Calvete*, 2005; *Ashton and Murray*, 2006a; *van den Berg et al.*, 2012; *Kaergaard and Fredsoe*, 2013a] with the exception of *Idier et al.* [2011] have found the existence of a critical angle for HAWI and, indeed, observations suggest that high-angle wave climates correlate with sandwaves existence [*Ashton et al.*, 2001; *Ashton and Murray*, 2006b; *Medellín et al.*, 2009; *Idier and Falqués*, 2014; *Kaergaard and Fredsoe*, 2013b]. However, to our best knowledge, the value of the critical angle has only been tested in the spit of Long Point (Lake Erie, Canada) by *Ashton* *and Murray* [2006b]. This site is characterised by a coastal stretch without sandwaves in between two stretches with sandwaves. The overall shoreline orientation is changing such that, under the same deep water wave angles, the incidence angles relative to the local shoreline exhibit spatial differences of about 25°. In addition, section 4.4 suggests that the bathymetric perturbation is prone to the existence of an absolute critical angle. *Ashton and Murray* [2006b] defined a dimensionless "instability index", Γ, which assesses the competition between diffusion and antidiffusion for a wave climate. This index depends on deep water wave height, period and direction and is based on the underlying assumption that the bathymetric contours are parallel to the shoreline, i.e., our P1 perturbation. When using the CERC formula, this index is antidiffusive ($\Gamma < 0$) if the weigthted proportion of angles θ larger than 42° is higher than those smaller than 42°. In other words, it is based on the absolute critical wave angle θ_{c0}, but not on the critical wave angle which also depends on D_c, A or T_p (in case of a P1 perturbation). *Ashton and Murray* [2006b] computed the local instability index along the spit and they found a good correlation with the existence or not of sandwaves, i.e., sandwaves show up when $\Gamma < 0$ and they are not present when $\Gamma > 0$. This is a clear indication that sandwaves form on that coast whenever deep water waves approach at angles greater than about 42° with respect to the shoreline.

Such value nearly equals the absolute critical angle θ_{c0} that we obtain for the P1 perturbation and using also the CERC formula. To assess the probability that the critical wave angle for Long Point spit coincides with the absolute critical angle, we use the probability function $p(\theta_c = \theta_{c0})$ introduced in section 3.3. This function depends on A, D_c and T_p. To estimate D_c and T_p, we use the wave hindcast [*Hubert*, 1992] of the WIS project of

USACE (data available at http://wis.usace.army.mil/). The analysis of the time series of hourly wave conditions at the station 92193 (42.48°N, −80.32°E, 20 m depth) over the period 1979-2014 provides a mean peak period of 3.7 s and a closure depth of 11.2 m using the formula of *Hallermeier* [1978]. It should be reminded that Lake Erie is very elongated such that the fetch at Long Point spit can be larger than 200 km. This explains the large obtained closure depth, together with a small mean peak wave period. For the estimation of A, we use the same bathymetric data as in section 4.4 and found values in the range $0.06 - 0.08$ m$^{1/3}$. With these values, a high probability, $p(\theta_c = \theta_{c0}) = 0.97$, is obtained, suggesting $\theta_c \approx \theta_{c0}$ on Long Point spit. The wave climate being not steady, $p(\theta = \theta_{c0})$ is computed also at each time step of the wave time series and a probability $p(\theta = \theta_{c0}) > 0.9$ during 70% of the time is obtained (meaning that $\theta_c \approx \theta_{c0}$ most of the time on Long Point spit). This would explain why *Ashton and Murray* [2006b] found a good spatial correlation between their instability index and the sandwave occurrence on this site.

In general, our grid experiment and the analysis of the results (see section 3.3) show that the probability to be in a configuration such that $\theta_c = \theta_{c0}$ is small when considering the range of all possible parameter values and that observing θ_{c0} (e.g., with a 0.95 probability, Figure 8) requires very specific conditions (small wave period and large closure depth). The initial purpose of the instability index developed by *Ashton and Murray* [2006a] was to provide general guidances rather than exact conditions for predicting shoreline stability/instability. However, the above analysis highlights that under certain conditions, this index should be more than a general guide: when negative, the index appears as a necessary (but not sufficient) condition for shoreline instability, but converge to sufficient condition for small wave period and/or large closure depth. This comment holds for a bathymetric perturbation corresponding to a profile shift (P1).

5. Conclusions

For the first time, a systematic model exploration of the relative contribution of wave conditions, shoreface shape and closure depth to self-organized shoreline sandwave generation is done. Since the analysis is based on the one-line approximation, a shape for the bathymetry associated with the sandwaves must be defined and the sensitivity to this shape is investigated. Two perturbation shapes are considered: one defined from a shift in the cross-shore equilibrium bathymetric profile, the other one defined from a linear seaward decay in bed level perturbation. Importantly, these definitions imply that the curvature of the depth contours cannot be larger than the one of the shoreline in the former case, whereas it can be larger in the latter case if $A^3/D_c\beta_s^2 < 1.48$ (assuming a Dean profile), i.e. if the shoreface slope is small enough and the closure depth and surf zone large enough.

As a consequence of these curvature properties, the critical wave angle for instability is highly sensitive to the shape of the perturbation. For a given profile shift perturbation, there is an absolute critical angle, $\theta_{c0} \approx 40 - 50°$, below which there is no instability for any condition (HAWI). Observing the absolute critical angle should be exceptional: the Long Point site is one example illustrating the required specific conditions (high-angle waves, small wave period and large closure depth). A bed level perturbation linearly decreasing in the offshore direction does not exhibit any absolute critical angle, such that, depending on the physical parameters, the critical angle can span the whole range $0 \leq \theta_c \leq 90°$ and instability can develop also for relatively low angles (LAWI). This is related to the amplitude of the bathymetric undulations being larger than that of the shoreline. The effect of two other perturbation shapes on the instability onset has also been analysed, confirming that the bathymetric perturbation and the related curvature of the depth contours play a key role in the instability onset, especially for low angles. In fact, the bed perturbation could be classified into two types: those with depth contour curvatures smaller or equal to the shoreline one, those with depth contour curvature that can be larger than the shoreline one offshore the breaking zone. The analysis of three shoreline sandwave sites suggests that both could exist in nature. This key effect, for the first time identified, explains some differences in the results of previous studies.

The main results of the exploration of the physical parameters are summarized in Table 3. Interestingly, some properties of shoreline instability are insensitive to the shape of the bathymetric perturbation: (1) the wave angle θ is the dominant parameter for the instability onset, (2) large D_c favours instability and reduces the critical wave angle θ_c, (3) the effect of T_p mainly increases with θ, (4) small T_p favours instability and decrease θ_c and (5) D_c and T_p have the largest effect on θ_c value. The most striking difference is the effect of the cross-shore profile which depends on the perturbation shape: while perturbations of type "profile shift" show little sensitivity to it, bed level perturbations linearly decreasing are highly sensitive to surf zone mean slope and bathymetric gradient, with large β_s and small A favouring instability.

The data produced in the present paper provide quantitative elements which could help to identify sites prone to shoreline sandwaves (at least in areas of low variability in the wave climate). In any case and thinking on future field work, the coasts the most prone to shoreline sandwaves are those characterized by high-angle waves, large closure depth and small wave periods. For relatively low angles, additional conditions for instability are a small enough bathymetric gradient of the shoreface and a large enough surf zone slope. For field studies, as the bathymetric anomaly associated with the sandwaves has a significant effect on the critical angle, it will be essential to analyse the existing bathymetric data (or undertake surveys), from the coast to the closure depth.

Notation

a Shoreline sandwave amplitude, m.

A Shoreface slope coefficient, $\mathrm{m}^{1/3}$.

α_b Wave angle at breaking, °.

β_s Surf zone slope.

C Horizontal slope of depth contours.

D Water depth, m.

D_0 Water depth of the unperturbed bathymetry, m.

D_c Closure depth, m.

f Shape function.

ϕ maximum angle between the perturbed bathymetric contour and the mean shoreline, °.

H Wave height, m.

H_b Wave height at breaking, m.

H_s Significant wave height, m.

K Shoreline sandwave wavenumber, m^{-1}.

L Shoreline sandwave wavelength, m.

p Probability.

p_s Ratio between a number of simulation for which instability develops and the number of total simulation, for a given set of parameters.

Q Longshore sediment flux, $\mathrm{m}^3\mathrm{s}^{-1}$.

R_{X_i} Ratio $(p_s(\max(X_i), \theta)+1)/(p_s(\min(X_i), \theta)+1)$.

σ Growth rate, s^{-1}.

T Wave period, s.

T_p Peak wave period, s.

θ Wave incidence angle, $^\circ$.

θ_c Critical wave incidence angle below which no shoreline sandwave develops, $^\circ$.

θ_{c0} Absolute critical wave incidence angle below which no shoreline sandwave develops whatever the physical parameters, $^\circ$.

y_b Cross-shore wave breaking position, m.

y_c Cross-shore position such that $D(y_c) = D_c$, m.

y_m Cross-shore location of the maximum bathymetric curvature, m.

y_s Cross-shore position of the shoreline, m.

z_b Seabed level, m.

Acknowledgments.

Funding from BRGM (ShorelineSW project) and the Spanish government (CTM2009-11892/IMNOBE and CTM2015-66225-C2-1/MUSA projects) are acknowledged. These projects have been cofunded by the E.U. (FEDER). The authors are grateful to F. Ardhuin, NOAA and USACE for providing respectively: the global wave hindcast data (available at ftp://ftp.ifremer.fr/ifremer/ww3/HINDCAST/GLOBAL/), the Lake Erie bathymetric contours (available at http://www.ngdc.noaa.gov/mgg/greatlakes/erie.html) and the Lake Erie wave hindcast data (available at http://wis.usace.army.mil/). The authors like also to thank D. Calvete for interesting discussions and technical support, B. Murray for a fruitful debate that has motivated the analysis of the bathymetric perturbation shape and F. Ribas for discussion on the Holsmlands Tange bathymetric anomaly. The referees are also gratefully acknowledged for their thorough review and useful advices.

References

Anthony, D., and J.O. Leth (2002), Large-scale bedforms, sediment distribution and sand mobility in the eastern North Sea of the Danish west coast, *Mar. Geol.*, *182*, 247263.

Ashton, A., and A. B. Murray (2006a), High-angle wave instability and emergent shoreline shapes: 1. Modeling of sand waves, flying spits, and capes, *J.Geophys.Res.*, *111*, F04,011,doi:10.1029/2005JF000,422.

Ashton, A., and A. B. Murray (2006b), High-angle wave instability and emergent shoreline shapes: 2. Wave climate analysis and comparisons to nature, *J.Geophys.Res.*, *111*, F04,012,doi:10.1029/2005JF000,423.

Ashton, A., A. B. Murray, and O. Arnault (2001), Formation of coastline features by large-scale instabilities induced by high-angle waves, *Nature*, *414*, 296–300.

Bender, C. J., and R. G. Dean (2003), Wave field modification by bathymetric anomalies and resulting shoreline changes: a review with recent results, *Coast. Eng.*, *49*, 125–153.

Coco, G., and A. B. Murray (2007), Patterns in the sand: From forcing templates to self-organization, *Geomorphology*, *91*(271-290).

Davidson-Arnott, R. G. D., and A. van Heyningen (2003), Migration and sedimentology of longshore sandwaves, Long Point, Lake Erie, Canada, *Sedimentology*, *50*, 1123–1137.

Dean, R. G. (1977), Equilibrium beach profiles: U.S. Atlantic and Gulf coasts, *Tech. rep.*, Delaware Univ., Delaware, U.S.A.

Dean, R. G. (1987), Coastal sediment processes: Toward engineering solutions, in *Coastal Sediments '87*, pp. 1–24, Am. Soc. of Civ. Eng.

Falqués, A. (2006), Wave driven alongshore sediment transport and stability of the Dutch coastline, *Coastal Eng.*, *53*, 243–254.

Falqués, A., and D. Calvete (2005), Large scale dynamics of sandy coastlines. Diffusivity and instability, *J. Geophys. Res.*, *110*(C03007), doi:10.1029/2004JC002587.

Falqués, A., F. Ribas, D. Idier, and J. Arriaga (2017), Formation mechanisms for self-organized kilometer-scale shoreline sand waves, *J. Geophys. Res. Earth Surf.*, *122*, doi:10.1002/2016JF003964.

Hallermeier, L. (1981), A profile zonation for seasonal sand beaches from wave climate, *Coastal Eng.*, *4* (3), 253–277.

Hallermeier, R. J. (1978), Uses for a calculated limit depth to beach erosion, in *Coastal Eng. 1978*, pp. 1493–1512, Am. Soc. of Civ. Eng.

Hothorn, T., and B. Everitt (2014), *A handbook of statistical analyses using R*, third ed., CRC press.

Hubert, J. M. (1992), User's guide to the wave information studies (wis) wave model: Version 2.0, *Tech. Rep. WIS Report 27*, US Army Corps of Engineers.

Idier, D., and A. Falqués (2014), How kilometric sandy shoreline undulations correlate with wave and morphology characteristics: preliminary analysis on the Atlantic coast of Africa, *Advances in Geosciences*, *39*, 55–60, doi:10.5194/adgeo-39-55-2014.

Idier, D., A. Falqués, B. G. Ruessink, and R. Garnier (2011), Shoreline instability under low-angle wave incidence, *J. Geophys. Res.*, *116* (F04031), doi:10.1029/2010JF001894.

Kaergaard, K., and J. Fredsoe (2013a), Numerical modeling of shoreline undulations part 1: Constant wave climate, *Coastal Eng.*, *75*, 64–76.

Kaergaard, K., and J. Fredsoe (2013b), Numerical modeling of shoreline undulations part 2: Varying wave climate and comparison with observations, *Coastal Eng.*, *75*, 77–90.

Kaergaard, K., J. Fredsoe, and S. B. Knudsen (2012), Coastline undulations on the West Coast of Denmark: Offshore extent, relation to breaker bars and transported sediment volume, *Coastal Eng.*, *60*, 109–122.

Komar, P. D. (1998), *Beach Processes and Sedimentation*, second ed., Prentice Hall, Englewood Cliffs, N.J.

Limber, P.W., P.N. Adams, and A.B. Murray (2017), Modeling large-scale shoreline change caused by complex bathymetry in low-angle wave climates, *Marine Geology*, *383*, doi:10.1016/j.margeo.2016.11.006.

Medellín, G., R. Medina, A. Falqués, and M. González (2008), Coastline sand waves on a low-energy beach at 'El Puntal' spit, Spain, *Mar. Geol.*, *250*, 143–156.

Medellín, G., A. Falqués, R. Medina, and M. González (2009), Sand waves on a low-energy beach at 'El Puntal' spit, Spain: Linear Stability Analysis, *J. Geophys. Res.*, *114*(C03022), doi:10.1029/2007JC004426.

Mei, C. C. (1989), *The Applied Dynamics of Ocean Surface Waves*, *Advanced Series on Ocean Engineering*, vol. 1, World Scientific, Singapore.

Metz, C. (1978), Basic principles of roc analysis, *Seminars in nuclear medicine*, *8*(4), 283–298.

Pierson, W. J., and L. Moskowitz (1964), A proposed spectral form for fully developed wind seas based on the similarity theory of s. a. kitaigorodskii., *J. Geophys. Res.*, *69*, 51815190.

Rascle, N., and F. Ardhuin (2013), A global wave parameter database for geophysical applications. part 2: Model validation with improved source term parameterization, *Ocean Modeling*, *70*(10), doi:10.1016/j.ocemod.2012.12.001.

Ribas, F., A. Falqués, H. E. de Swart, N. Dodd, R. Garnier, and D. Calvete (2015), Understanding coastal morphodynamic patterns from depth-averaged sediment concentration, *Rev. Geophys.*, *53*, doi:10.1002/2014RG000457.

Riggs, S. R., W. J. Cleary, and S. W. Snyder (1995), Influence of inherited geologic framework on barrier shoreface morphology and dynamics, *Marine Geology*, *126*(1), 213–234.

Ruessink, B. G., and M. C. J. L. Jeuken (2002), Dunefoot dynamics along the dutch coast, *Earth Surf. Process. Landforms*, *27*, 1043–1056.

Ryabchuk, D., I. Leont'yev, A. Sergeev, E. Nesterova, L. Sukhacheva, and V. Zhamoida (2011), The morphology of sand spits and the genesis of longshore sand waves on the coast of the eastern Gulf of Finland, *Baltica*, *24*(1), 13–24.

Uguccioni, L., R. Deigaard, and J. Fredsoe (2006), Instability of a coastline with very oblique wave incidence, in *Coastal Eng. 2006*, pp. 3542–3553, World Scientific.

Valvo, L. M., A. B. Murray, and A. Ashton (2006), How does underlaying geology affect shoreline change? An initial model investigation, *J. Geophys. Res. Earth Surf.*, *111*(F02025), doi:10.1029/2005JF000340.

van den Berg, N., A. Falqués, and F. Ribas (2012), Modelling large scale shoreline sand waves under oblique wave incidence, *J. Geophys. Res.*, *117*(F03019), doi:10.1029/2011JF002177.

Wright, L. D., and A. D. Short (1984), Morphodynamic variability of surf zones and beaches: A synthesis, *Mar. Geol.*, *56*, 93–118.

Table 1. Design of computer experiments. The range (Min to Max), the sampling step (Δ) and the grid size (N) are provided for each of the following input parameters used for the stability analysis computations done with the 1D-morfo model: wave angle θ, surf zone slope β_s, shoreface slope coefficient A, closure depth D_c, wave height H_s, wave period T_p.

	θ (°)	β_s	A ($m^{1/3}$)	D_c (m)	H_s (m)	T_p (s)
Min	0	0.01	0.05	2.5	0.25	4
Max	85	0.5	0.3	27.5	4	16
Δ	5	0.01 to 0.1	0.05 to 0.1	2.5	0.25	1
N	18	16	4	6	16	13

Table 2. Regression coefficients of the logistic regression in dimensional and normalized (*) space of the parameters X_i, for the perturbation shapes P1 (profile shift) and P2 (linear decay of bed level perturbation). The normalized space corresponds to X_i parameters scaled between 0 and 1. "NS" refers to non significant effect.

f	Coef. value	a_0	a_{β_s}	a_A	a_{D_c}	a_{H_s}	a_{T_p}
P1	Dimensional	9.35	NS	14.4	0.589	NS	-3.59
	Normalized	-2.8	NS	3.6	14.8	NS	-43.1
P3	Dimensional	-0.32	36.02	-29.46	0.25	-0.62	NS
	Normalized	-0.94	17.65	-7.37	6.40	-2.32	NS

Table 3. Results synthesis for the P1 and P2 perturbation shapes in terms of probability of shoreline development (p_s), relative effect of the physical parameters versus the wave angle (R_X), probability that the critical angle is either equal to the absolute critical angle $p(\theta_c = \theta_{c0})$ or does not exist ($p(\theta_c \nexists)$), and the critical angle itself. The trend of these 5 types of results are given versus the wave angle θ, the surf zone slope β_s, the shoreface slope coefficient A, the closure depth D_c, the wave height H_s and wave period T_p. The +,=,− symbols mean positive effect, no effect, negative effect, respectively. * indicates dominant parameters. N.C. yields for "Not Concerned". The underline cells are cells showing similar conclusion for both the P1 and P2 perturbations.

f	Indicator	θ	β_s	A	D_c	H_s	T_p
P1	p_s	$\underline{+^*}$	$=$	$+$	$\underline{+^*}$	$\underline{=}$	$\underline{-^*}$
	R_X	N.C.	$\lvert\rightarrow\rvert$	$\lvert\nearrow\rvert$	$\lvert\nearrow\rvert$	$\lvert\rightarrow\rvert$	$\underline{\lvert\nearrow\rvert}$
	$p(\theta_c = \theta_{c0})$	N.C.	$=$	$+$	$\underline{+^*}$	$=$	$-^*$
	θ_c	N.C.	$=$	$-$	$\underline{-^*}$	$=$	$\underline{+^*}$
P2	p_s	$\underline{+^*}$	$+^*$	$-$	$\underline{+^*}$	$\underline{-}$	$\underline{-}$
	R_X	N.C.	$\lvert\searrow\rvert$	$\lvert\searrow\rvert$	$\lvert\searrow\rvert$	$\lvert\searrow\rvert$	$\underline{\begin{array}{c}\lvert\nearrow\rvert \\ \lvert\searrow\rvert\end{array}}$
	$p(\theta_c \nexists)$	N.C.	$+^*$	$-^*$	$\underline{+^*}$	$-$	$=$
	θ_c	N.C.	$-$	$+$	$\underline{-^*}$	$+$	$\underline{+^*}$

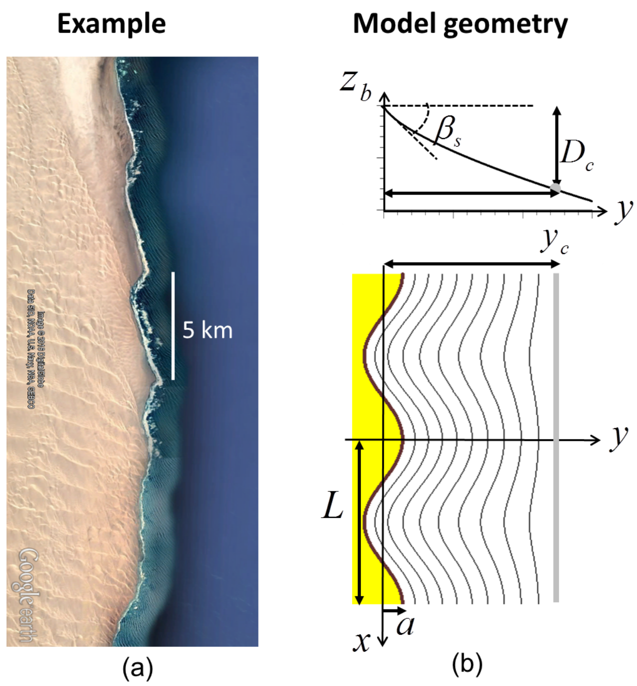

Figure 1. (a) Shoreline sandwave example (location: 23.8 ° N, 14.5° E) and (b) model geometry (cross and top view).

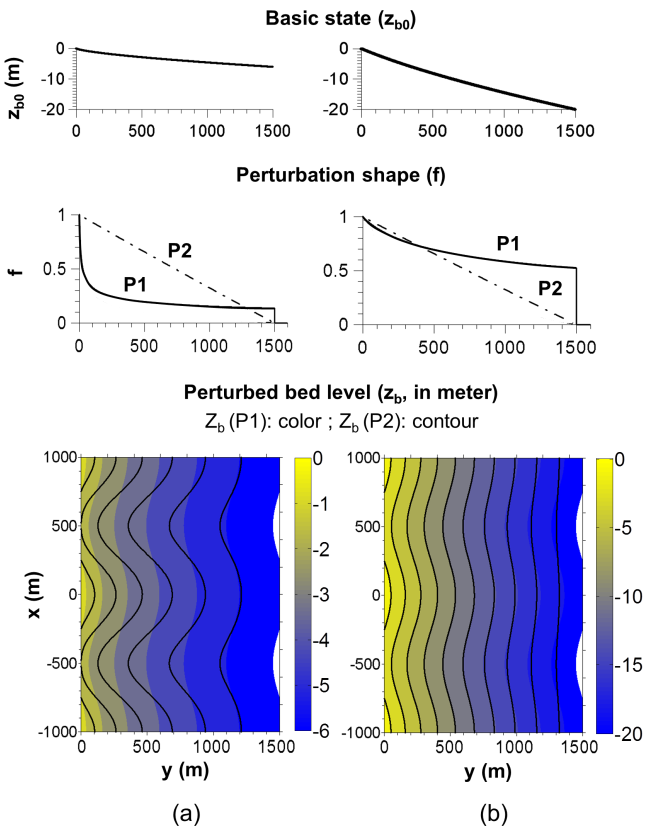

Figure 2. Basic state (cross-shore), perturbation shapes (cross-shore) and perturbed bed level (plan view) for two basic profiles: (a) $A = 0.047$ m$^{1/3}$ and (b) $A = 0.190$ m$^{1/3}$, with $\beta_s = 0.02$ for both profiles. In addition, the shown perturbations are such that D_c equals 6 m and 20 m for cases (a) and (b), respectively. The corresponding Ω value is 0.043 (a) and 0.86 (b).

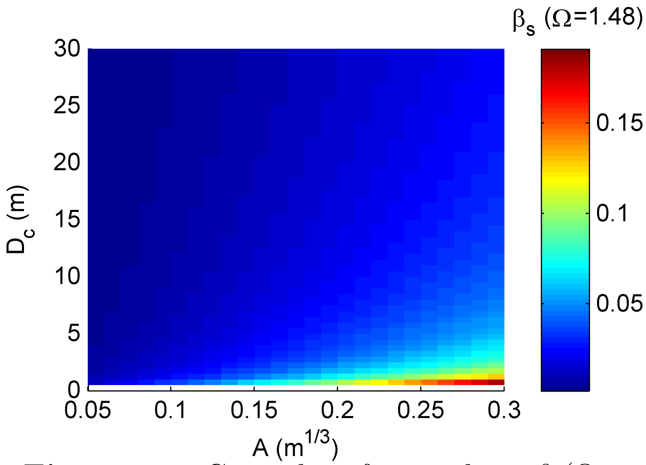

Figure 3. Critical surf zone slope $\beta_s(\Omega = 1.48)$ for given values of the closure depth D_c and shoreface slope coefficient A. For given values of D_c and A, a necessary condition for low-angle instabilities is $\beta_s > \beta_s(\Omega = 1.48)$

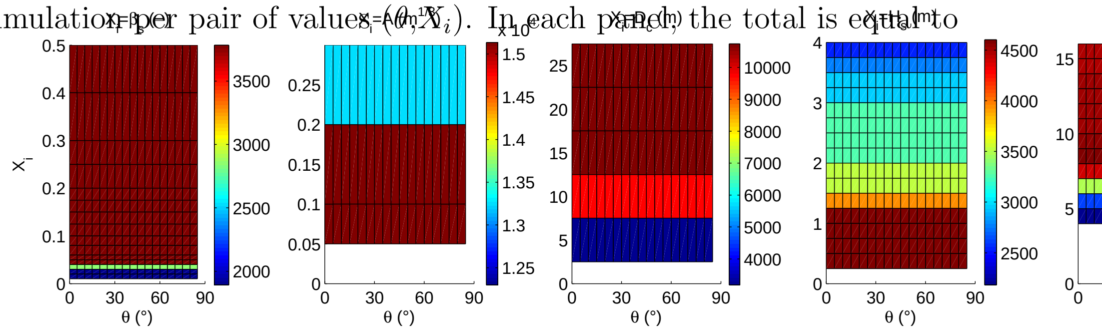

Figure 4. Number of simulation per pair of values (θ, X_i). In each panel, the total is equal to 1 004 652.

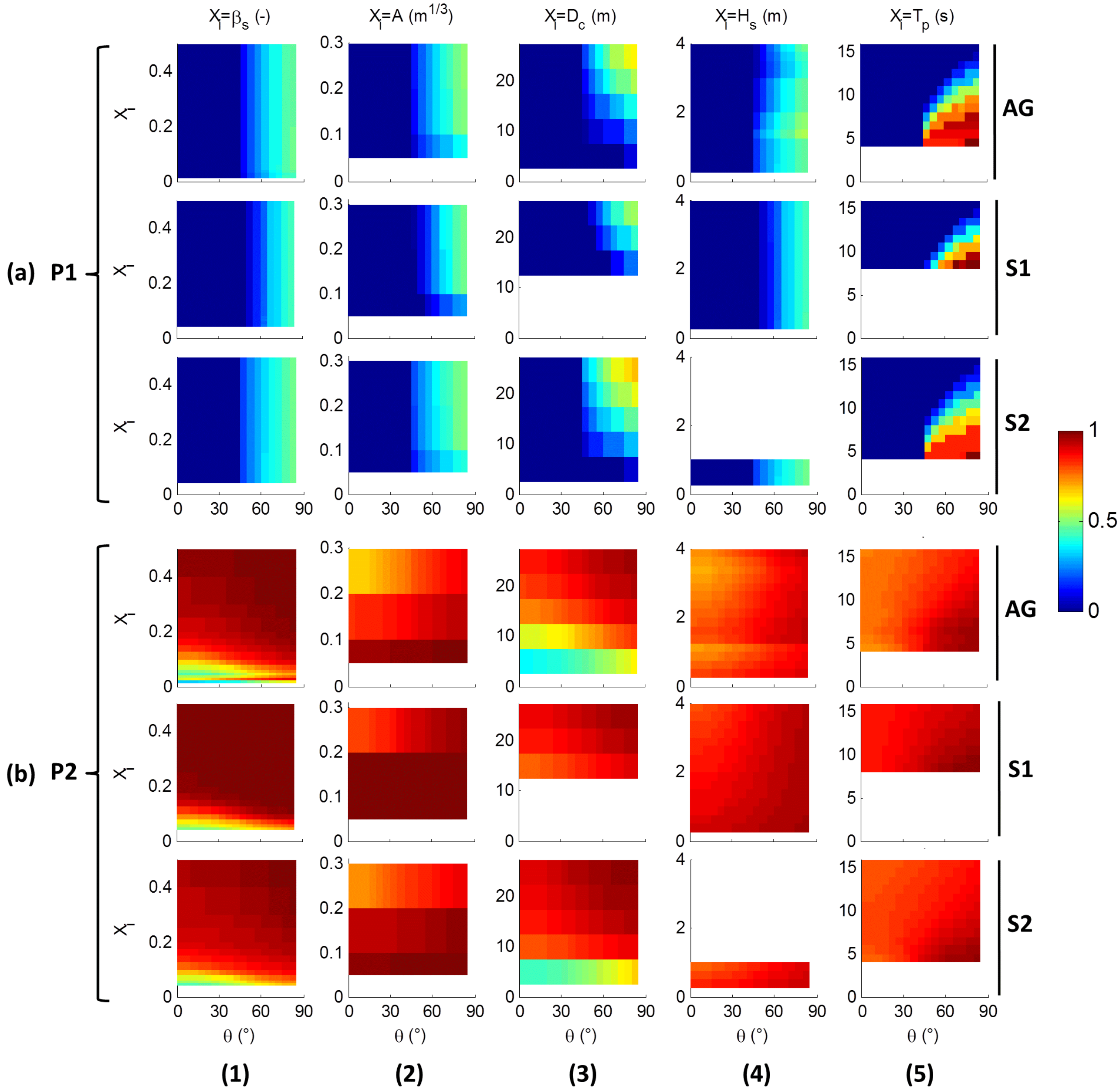

Figure 5. Probability $p_s(\theta, X_i)$ of shoreline sandwave development for the P1 (a) and P2 (b) perturbation shapes, and for the "all grid" experiment (AG), the subset 1 (S1) and the subset 2 (S2). $p_s(\theta, X_i)$ is equal to n_i/n_t with n_i the number of simulations for which instability develops and n_t the total number of simulation, n_i and n_t being computed over the experiment subset (θ, X_i). For instance, $p_s(\theta = 30°, \beta_s = 0.2) = n_i/n_t$ with n_i and n_t computed over the experiment subset $(\beta_s = 0.2, A, D_c, H_s, T_p, \theta = 30°)$. On the "AG" plots, some discontinuities can be observed. They are related with the non-uniformity of the grid experiment (see section 2.3). For instance, the discontinuity observed on panel b1 is due to the constraint C2, while the

discontinuities observed on panel b4 are due to both constraints C1 and C3.

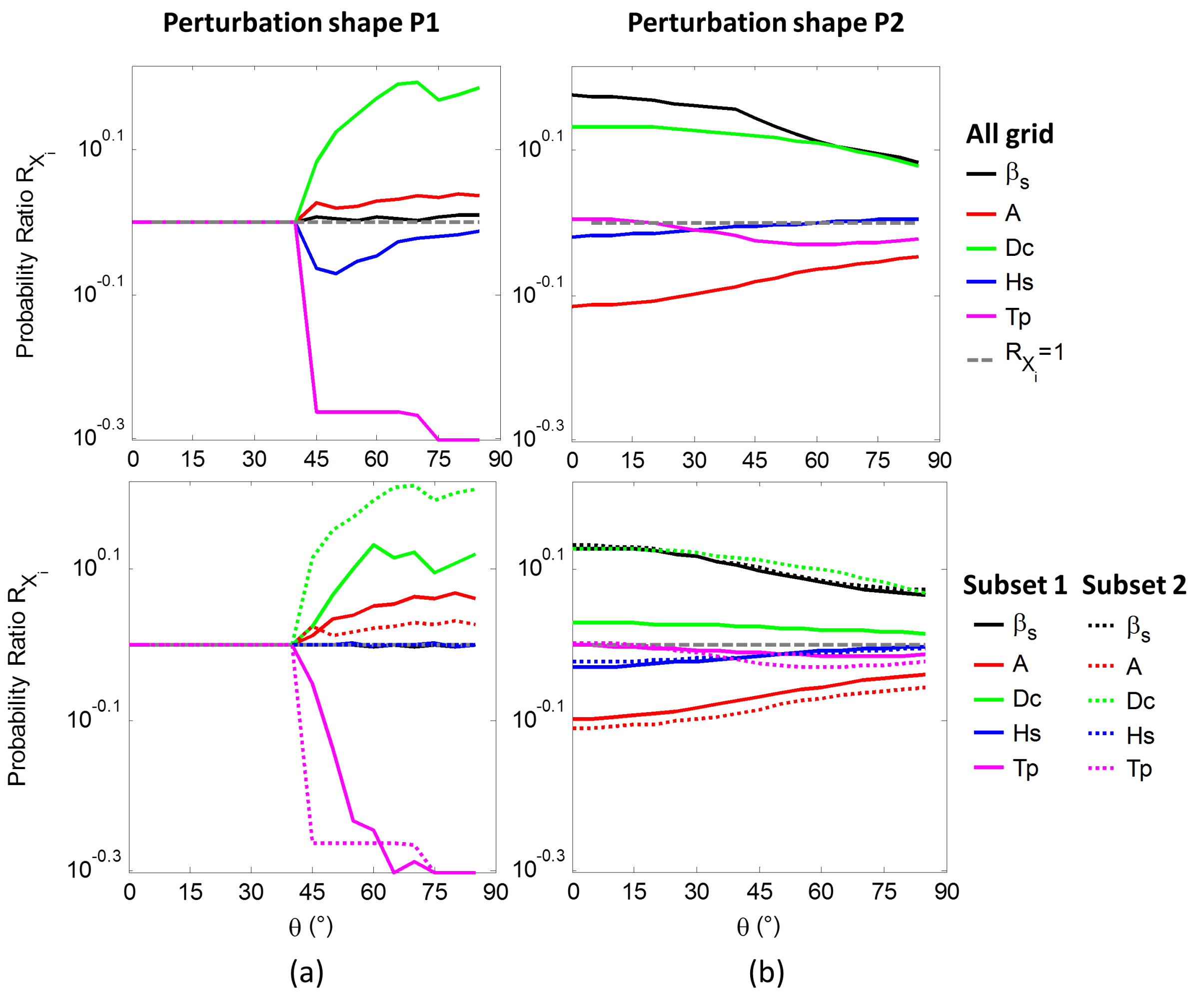

Figure 6. Probability Ratio R_{X_i} versus wave angle θ considering each parameter X_i, and for perturbation shapes P1 (a) and P2 (b). Top panel: R_{X_i} is computed using the entire grid experiment results ("All grid"). Bottom panel: R_{X_i} is computed using the subsets 1 and 2 (described in section 2.3) such that, within each subset, for any parameter X_i, exactly the same combinations of parameters X_j are considered with $j \neq i$. This figure shows how the effect of each parameter varies with the wave incidence angle: a decrease (increase) in $|R_{X_i} - 1|$ means that the effect of the X_i parameter decreases (increases) with the angle.

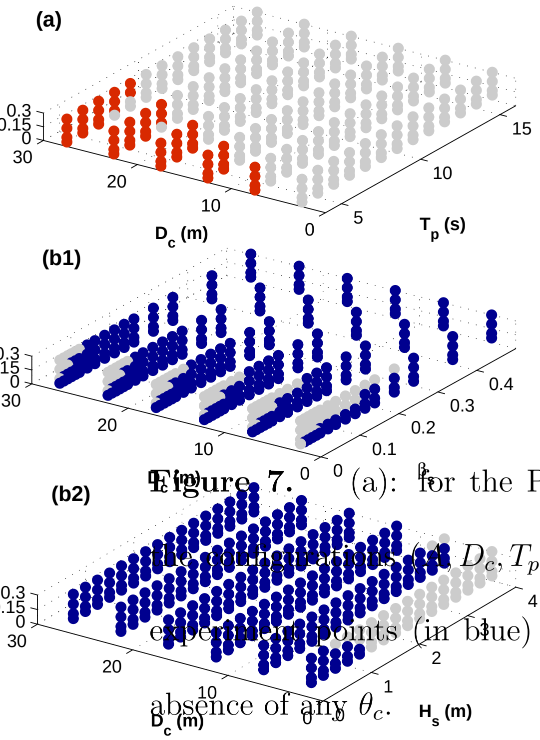

Figure 7. (a): for the P1 perturbation, grid experiment points (in red) corresponding to the configurations (A, D_c, T_p) leading to $\theta_c = \theta_{c0}$. (b1 and b2): for the P2 perturbation, grid experiment points (in blue) corresponding to the configurations (β_s, A, D_c, H_s) leading to the absence of any θ_c.

Figure 8. D_c at a probability $p(\theta_c = \theta_{c0}) = 0.95$ (Equation 12) plotted in the parameter space (T_p, A). The red and black lines indicate the 10 m and 30 m isovalue contours of D_c, respectively.

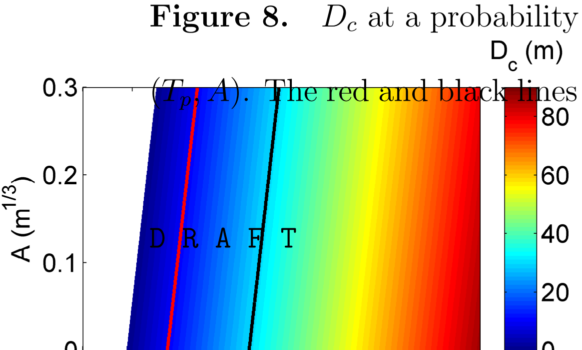

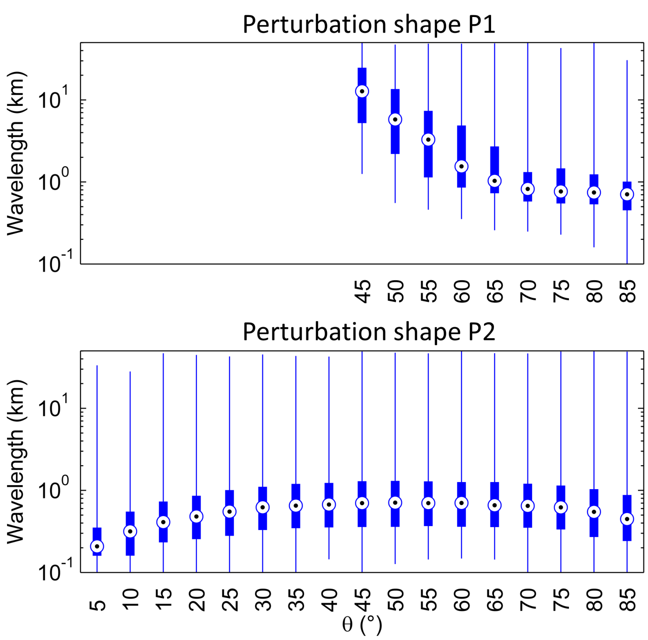

Figure 9. Boxplot of wavelength L of the Linearly Most Amplified modes, for the entire grid experiment, i.e. 55814 runs per wave direction θ: median (circle), 0.25 and 0.75 quantiles (vertical bar), and values above the 0.75 and below the 0.25 quantiles (vertical line).

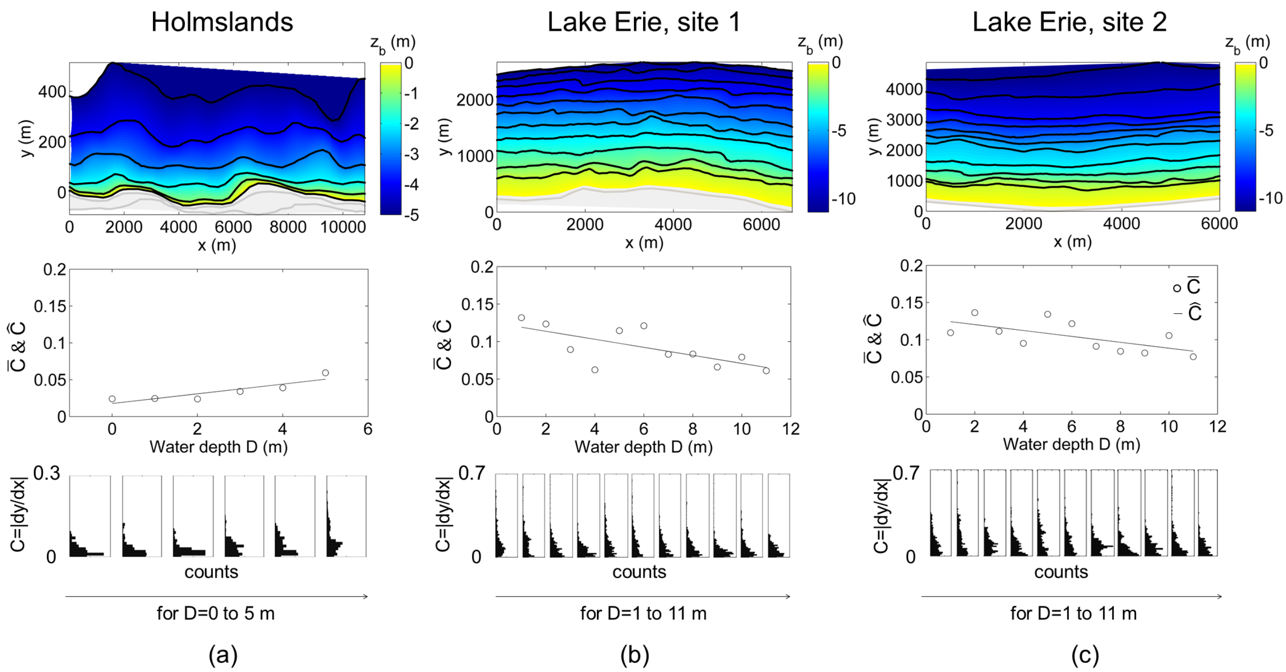

Figure 10. Bed level contours, bathymetric curvature indicators ($\bar{C}$, $\hat{C}$), and distribution of horizontal slope of depth contours ($C(D,x) = |dy/dx|$) versus the water depth for the Holmslands site (a), the distal end (b) and the toe (c) of the Lake Erie Long Point spit. Depths contours are plotted every meter. The black contours are used in the curvature analysis. For the Holmsland Tange site, the depths contours have been digitized on Figure 12 of [*Kaergaard et al.*, 2012]. For the Long Point sites, the contours come from the NOAA database. The coloured surface has been obtained by interpolation (natural neighbour method) of the plotted bathymetric contours. In the white area, the natural neighbour provides no bathymetric value. $C(D,x)$ is computed along each bathymetric contour of depth D and every 5 m in the x-direction. $\bar{C}(D)$ is the mean of $C(D,x)$ for the depth D, i.e. $\bar{C}(D) = (1/n_x)\sum_{i=1}^{n_x} C(D,x_i)$. $\hat{C}(D)$ is obtained by linear regression of $C(D,x)$.

Figure 1.

Example **Model geometry**

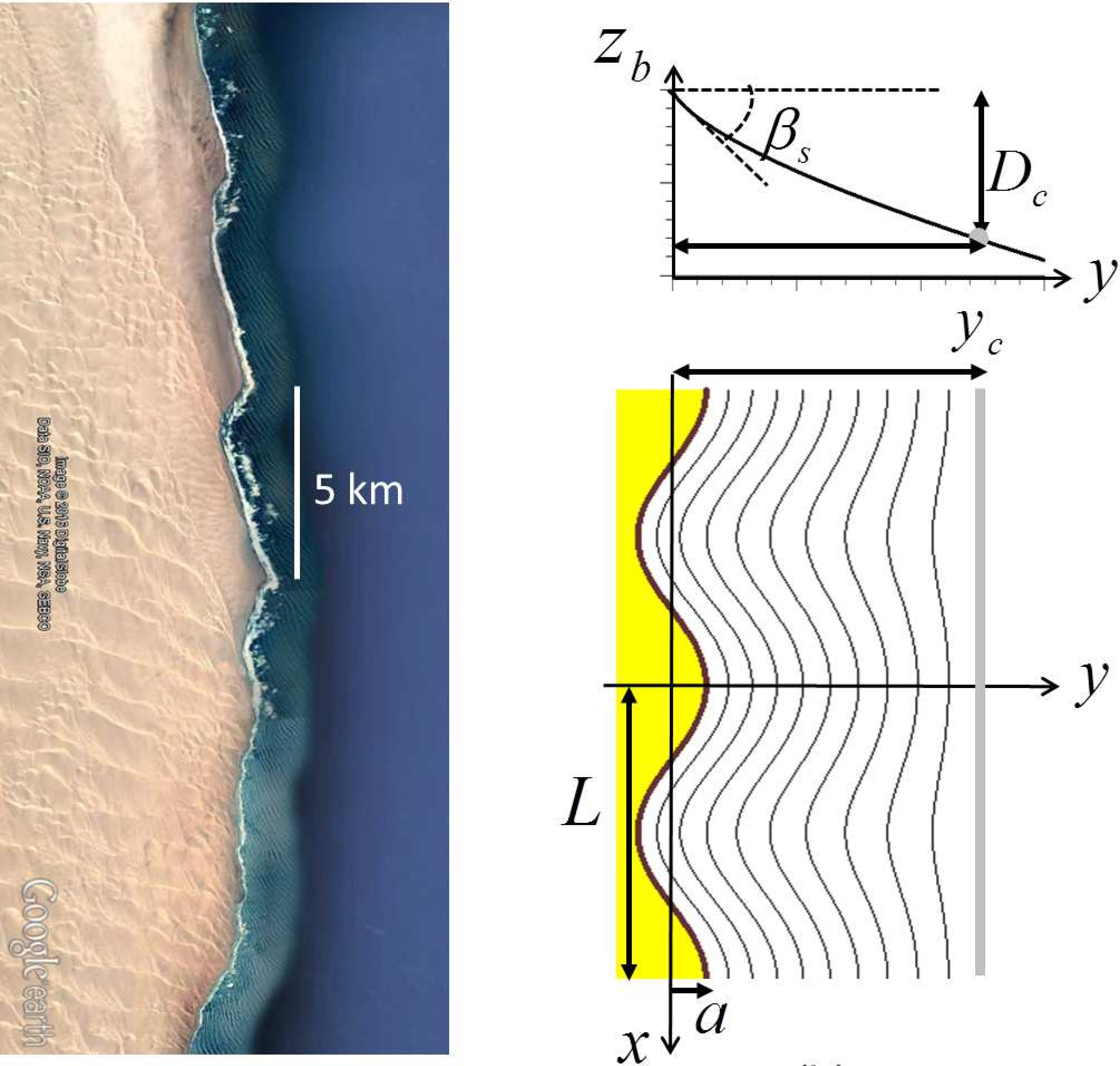

(a) (b)

Figure 2.

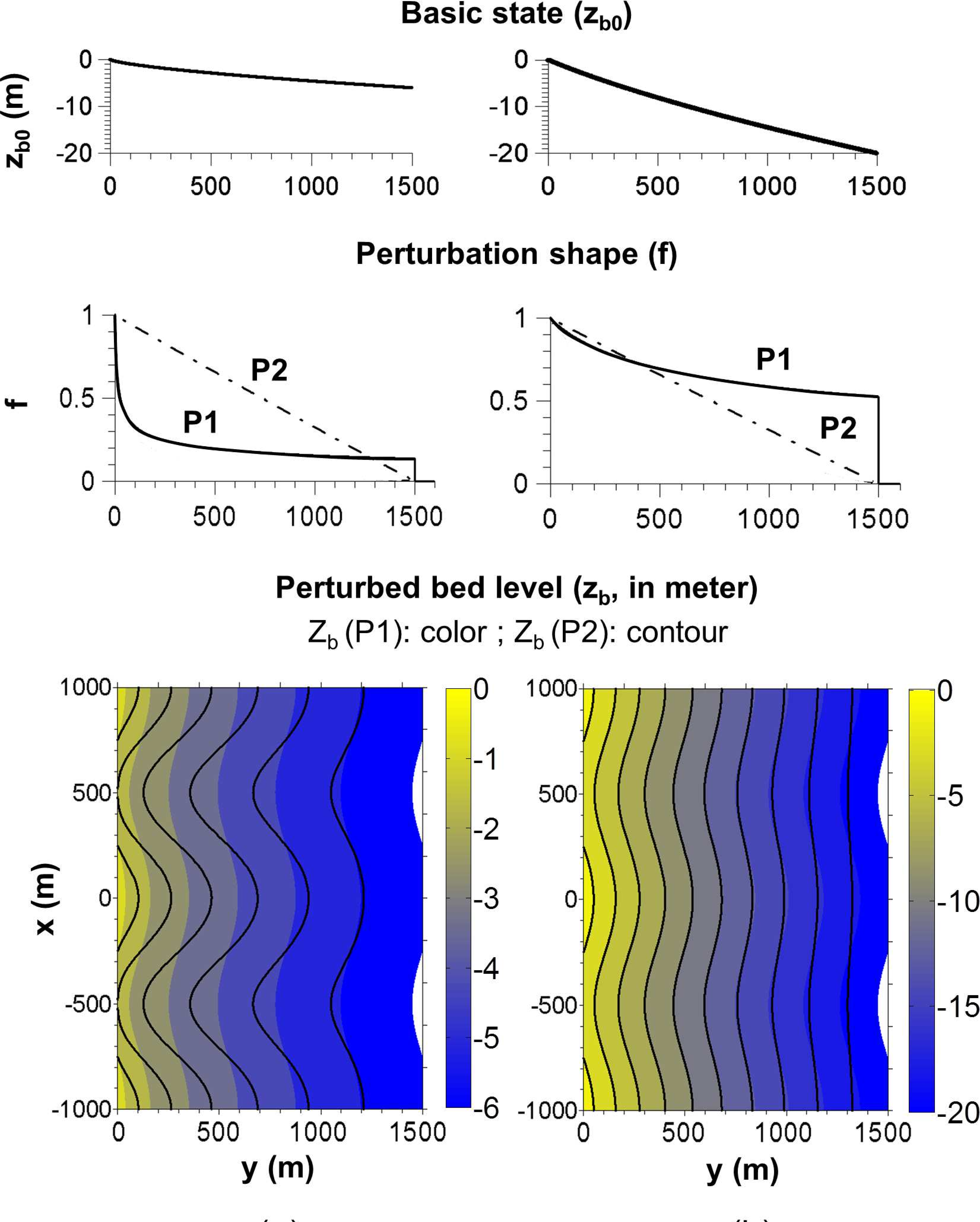

Basic state (z_{b0})
z_{b0} (m)
0
-10
-20
0
500
1000
1500
Perturbation shape (f)
f
1
0.5
0
P1
P2
Perturbed bed level (z_b, in meter)
Z_b (P1): color ; Z_b (P2): contour
x (m)
1000
500
0
-500
-1000
y (m)
-1
-2
-3
-4
-5
-6
-15

(a) (b)

Figure 3.

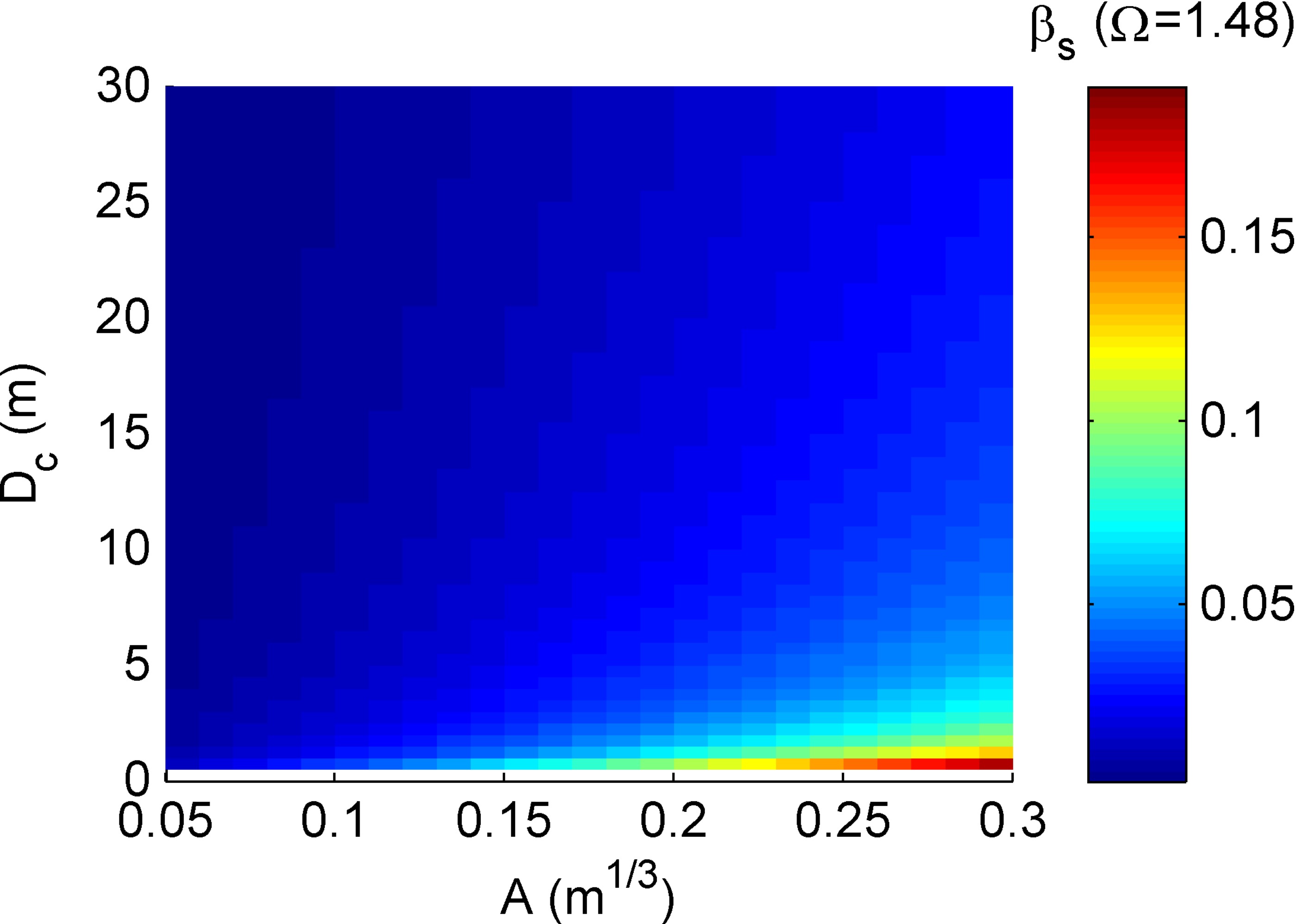

β_s (Ω=1.48)
30
25
20
15
10
5
0
D_c (m)
0.05
0.1
0.15
0.2
0.25
0.3
A ($m^{1/3}$)
0.15
0.1
0.05

Figure 4.

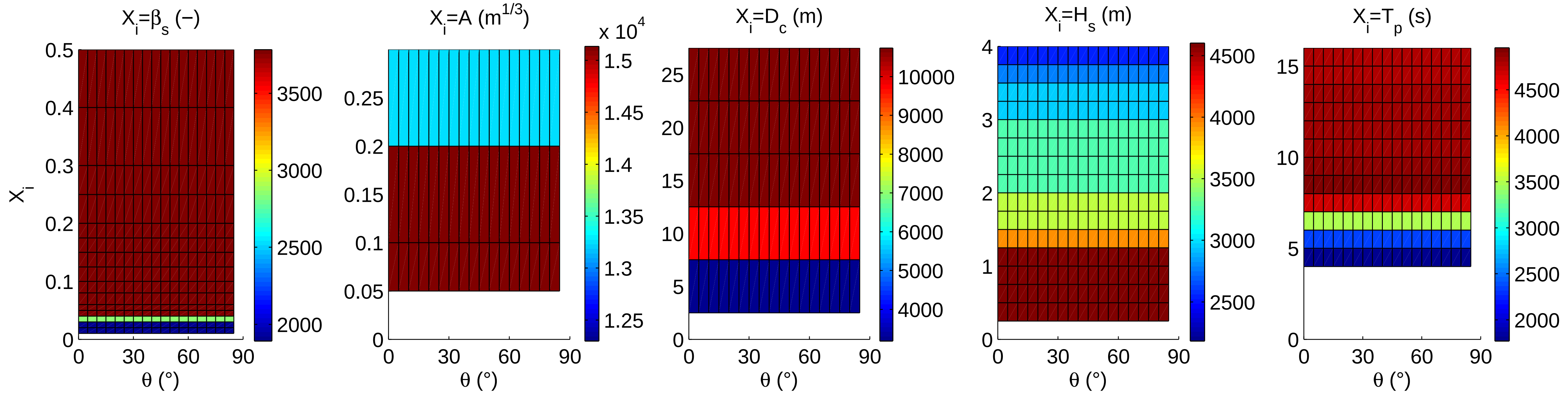

$X_i=\beta_s$ (−)
$X_i=A$ ($m^{1/3}$)
$X_i=D_c$ (m)
$X_i=H_s$ (m)
$X_i=T_p$ (s)
X_i
θ (°)
x 10^4

Figure 5.

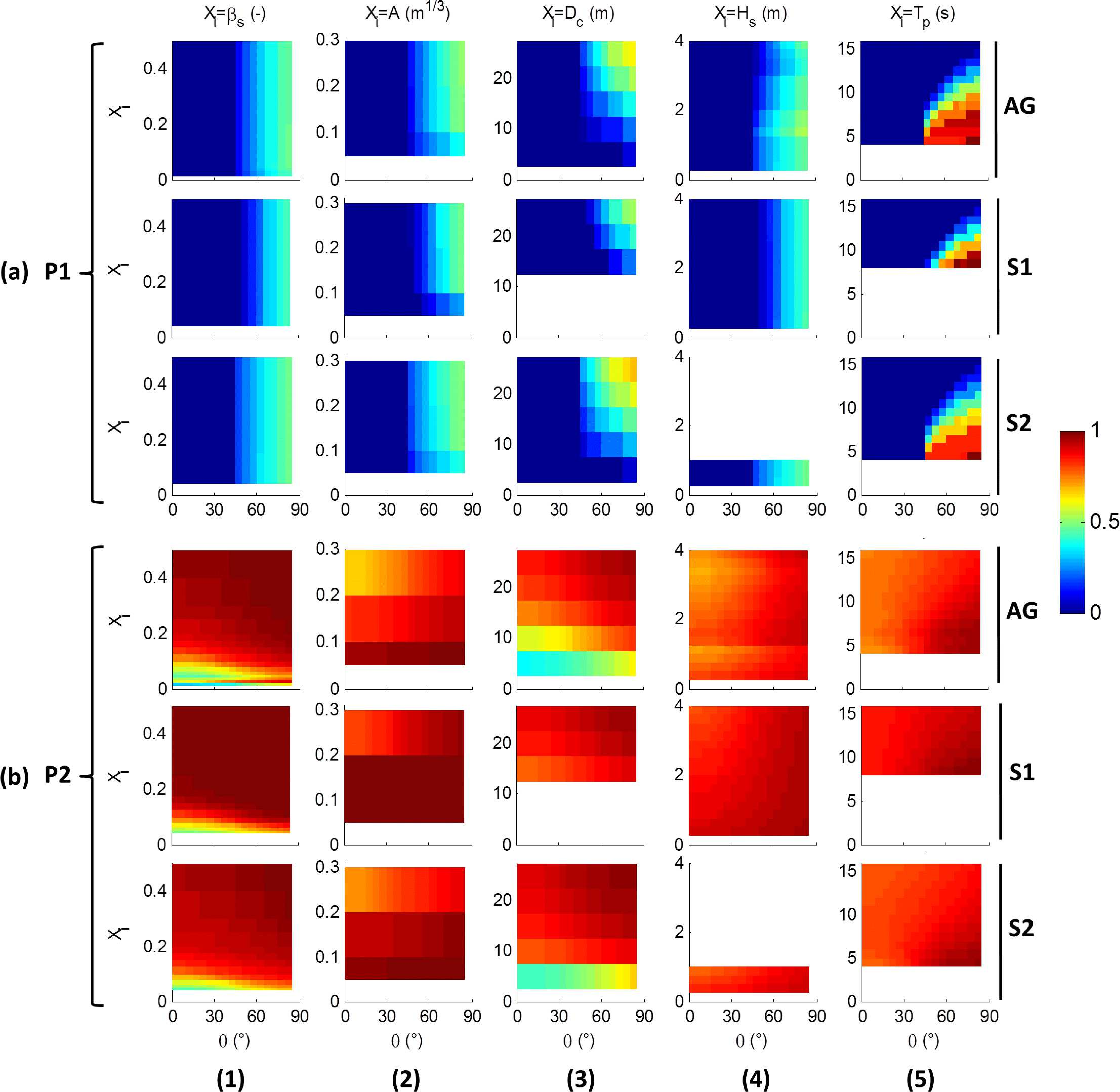

$X_i=\beta_s$ (-)
$X_i=A$ ($m^{1/3}$)
$X_i=D_c$ (m)
$X_i=H_s$ (m)
$X_i=T_p$ (s)
(a) P1
(b) P2
AG
S1
S2
X_i
θ (°)
(1)
(2)
(3)
(4)
(5)

Figure 6.

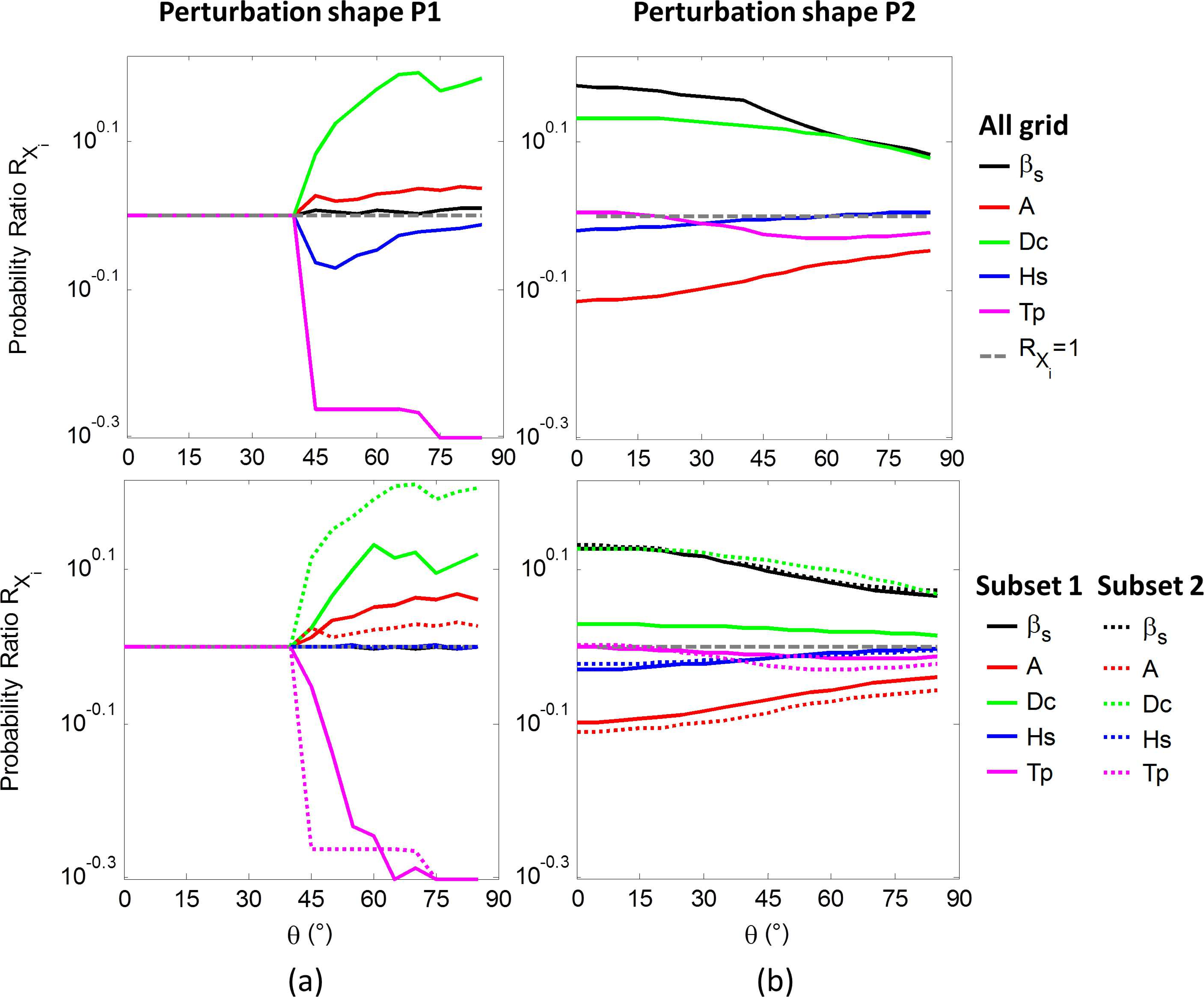

Perturbation shape P1
Perturbation shape P2
Probability Ratio R_{X_i}
$10^{0.1}$
$10^{-0.1}$
$10^{-0.3}$
0 15 30 45 60 75 90
θ (°)
All grid
β_s
A
Dc
Hs
Tp
$R_{X_i}=1$
Subset 1
Subset 2
(a)
(b)

Figure 7.

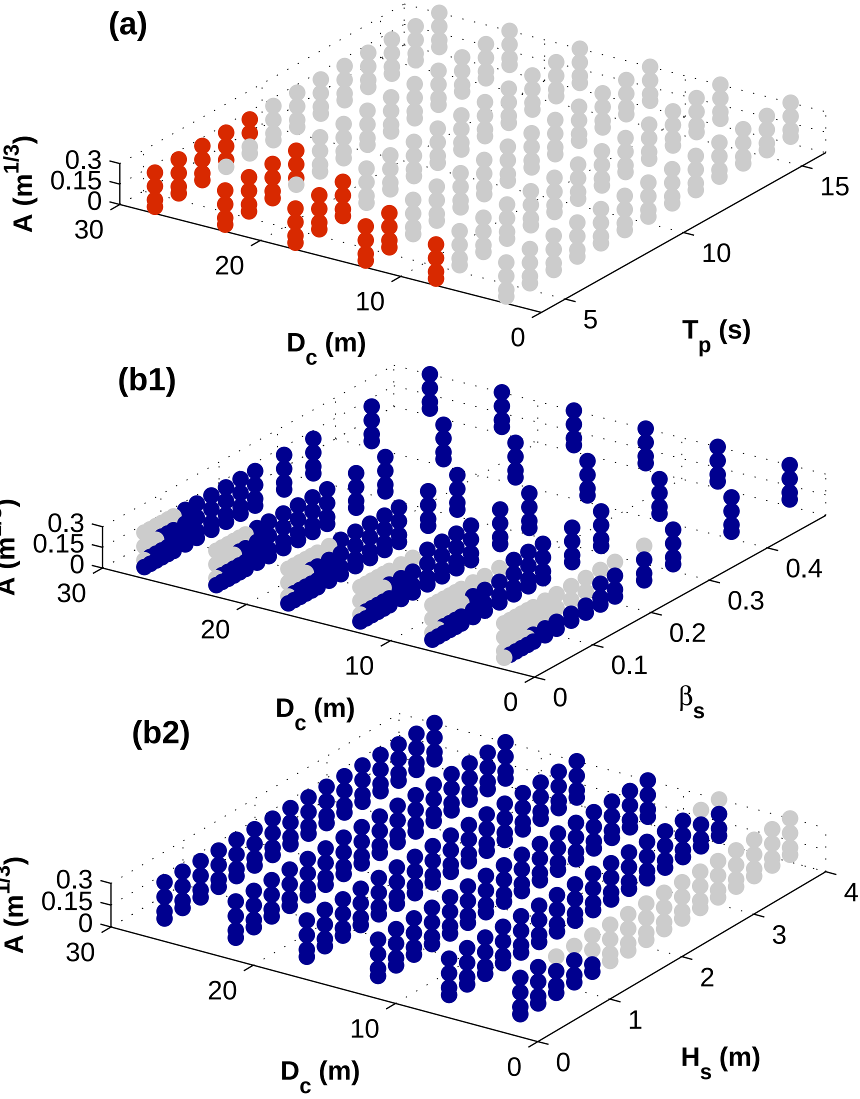
(a)
A ($m^{1/3}$)
0.3
0.15
0
30
20
10
0
D_c (m)
5
10
15
T_p (s)
(b1)
A ($m^{1/3}$)
0.3
0.15
0
30
20
10
0
D_c (m)
0
0.1
0.2
0.3
0.4
β_s
(b2)
A ($m^{1/3}$)
0.3
0.15
0
30
20
10
0
D_c (m)
0
1
2
3
4
H_s (m)

Figure 8.

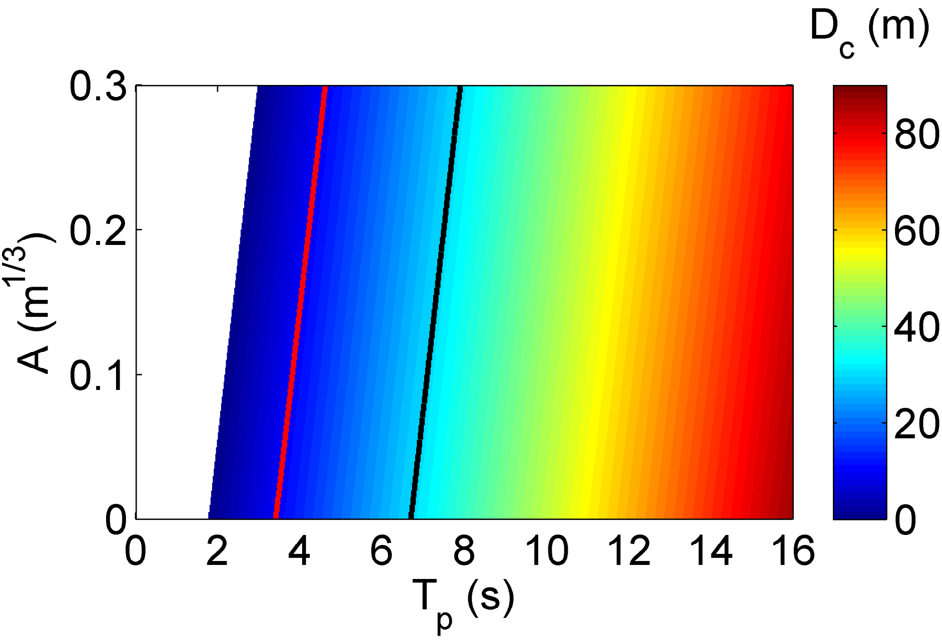

D_c (m)
0.3
0.2
0.1
0
A (m^1/3)
0
2
4
6
8
10
12
14
16
T_p (s)
80
60
40
20
0

Figure 9.

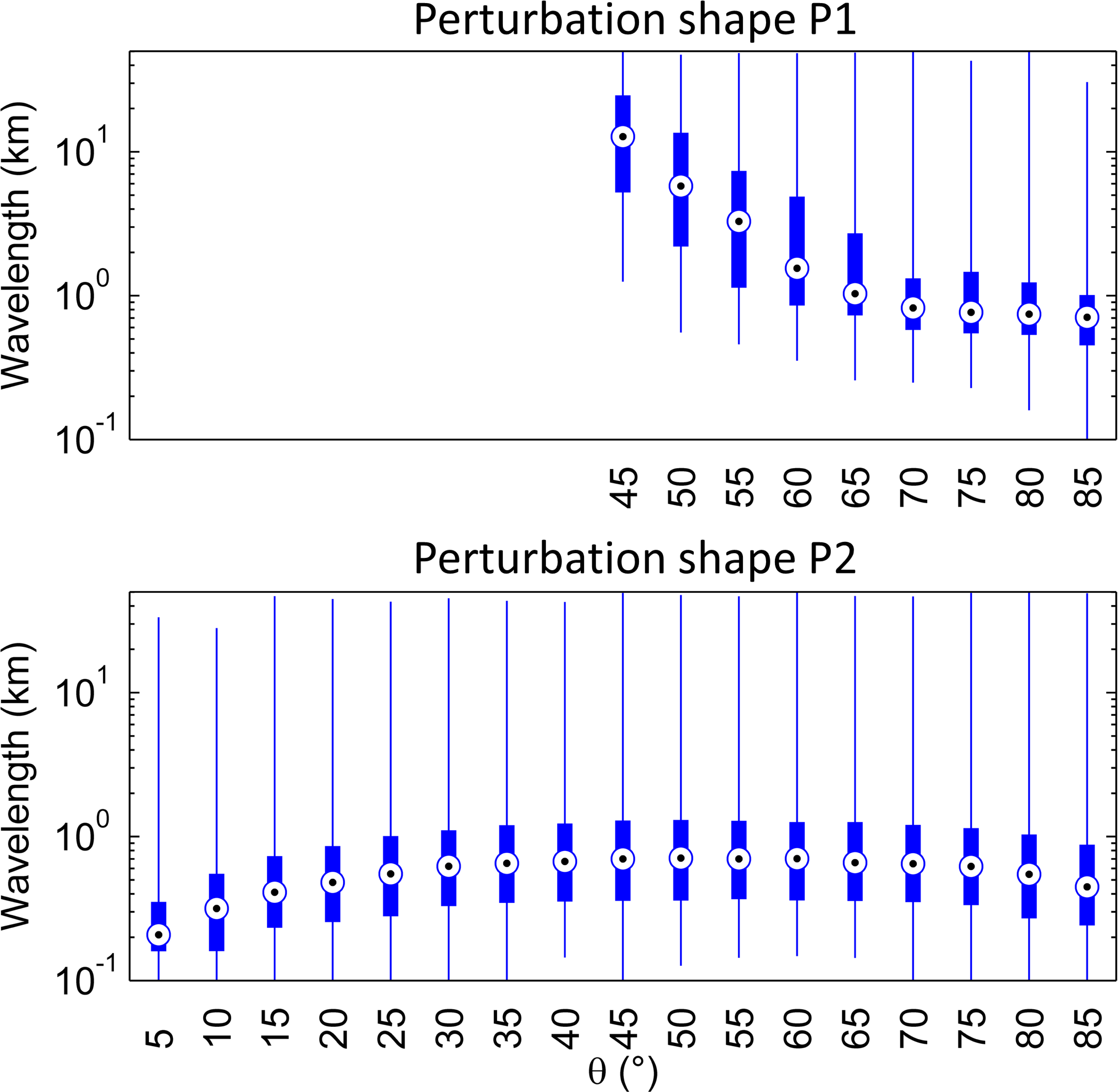

Perturbation shape P1
Wavelength (km)
10^1
10^0
10^{-1}
45
50
55
60
65
70
75
80
85
Perturbation shape P2
Wavelength (km)
10^1
10^0
10^{-1}
5
10
15
20
25
30
35
40
45
50
55
60
65
70
75
80
85
θ (°)

Figure 10.

Holmslands
Lake Erie, site 1
Lake Erie, site 2
z_b (m)
y (m)
x (m)
$\bar{C}$ & $\hat{C}$
Water depth D (m)
C=|dy/dx|
counts
for D=0 to 5 m
for D=1 to 11 m
for D=1 to 11 m
(a)
(b)
(c)